Research Square

Preprints are preliminary reports that have not undergone peer review.
They should not be considered conclusive, used to inform clinical practice,
or referenced by the media as validated information.

Subsurface Elastic Heterogeneity Across the Palolo Fault Revealed by HVSR-Derived Shear-Wave Velocity Models

Zalsa Nabila HR
Hasanuddin University
Valensya Arruan Silomba
Hasanuddin University
Nurul Maghfirah
Hasanuddin University
Samida Danda
Hasanuddin University
Andri Moh. Wahyu Laode
andriwahyu@unhas.ac.id
Hasanuddin University
Muhammad Altin Massinai
Hasanuddin University
Muh. Farid Wajedy
Hasanuddin University
Sofian Sofian
Meteorological, Climatological, And Geophysical Agency

Research Article

Keywords: HVSR, Shear-wave velocity, Subsurface heterogeneity, Fault-related deformation, Velocity architecture, Palolo Fault

Posted Date: September 7th, 2026

DOI: https://doi.org/10.21203/rs.3.rs-10844213/v1

License: This work is licensed under a Creative Commons Attribution 4.0 International License.
Read Full License

Additional Declarations: No competing interests reported.

Subsurface Elastic Heterogeneity Across the Palolo Fault Revealed by HVSR-Derived Shear-Wave Velocity Models

[1]Zalsa Nabila HR, [1,2]Valensya Arruan Silomba, [1,2]Nurul Maghfirah, [1]Samida Danda, [1*]Andri Moh Wahyu Laode, [1]Muhammad Altin Massinai, [1]Muh. Farid Wajedy, [3]Sofian

[1]Department of Geophysics, Faculty of Mathematics and Natural Science,
Hasanuddin University, South Sulawesi 90245, Indonesia
[2]Laboratory of Solid Geophysics, Faculty of Mathematics and Natural Science,
Hasanuddin University, South Sulawesi 90245, Indonesia
[3]Meteorology, Climatology and Geophysical Agency, Palu, Indonesia

*Corresponding author:
Andri Moh. Wahyu Laode
ORCiD: https://orcid.org/0009-0005-6155-1169
e-mail: andriwahyu@unhas.ac.id

Abstract

Fault-related deformation can produce strong lateral and vertical heterogeneity in near-surface elastic properties, yet its expression in shallow shear-wave velocity architecture remains poorly constrained where surface evidence is limited. This study investigates subsurface heterogeneity across the Palolo Fault in the Bora geothermal area, Central Sulawesi, Indonesia, by integrating ambient vibration measurements, Horizontal-to-Vertical Spectral Ratio (HVSR) analysis, and shear-wave velocity (Vs) inversion. Ambient vibration data from 25 stations distributed along two survey lines were processed to derive dominant frequency (f_0), peak amplitude (A_0), seismic vulnerability index (Kg), and one-dimensional Vs profiles. HVSR curves were inverted using the Neighborhood Algorithm, and the resulting station-based velocity models were integrated through ordinary Kriging to construct two-dimensional Vs sections. The HVSR results show marked spatial variability, with dominant frequencies of 0.57–7.54 Hz along Line A and 0.55–2.62 Hz along Line B. Inversion misfits range from 0.03 to 0.08, indicating close agreement between observed and theoretical HVSR responses. The velocity models reveal low-Vs near-surface materials (<500 m/s), intermediate velocities of 500–1500 m/s, and deeper high-Vs materials (>1500 m/s), with pronounced lateral changes in sediment thickness and bedrock geometry. A thickened low-velocity zone occurs around SP_A11–SP_A15, while Line B shows localized thickening near SP_B04–SP_B06. Several abrupt velocity discontinuities and vertically persistent low-velocity corridors may indicate localized fault-related deformation, although lithological variation, weathering, and interpolation effects cannot be excluded. The results demonstrate that HVSR-derived Vs architecture can provide useful constraints on concealed structural heterogeneity and deformation patterns along active faults.

Keywords: HVSR; Shear-wave velocity; Subsurface heterogeneity; Fault-related deformation; Velocity architecture; Palolo Fault

1 Introduction

Fault zones are mechanically complex geological systems that evolve through repeated episodes of tectonic deformation, producing substantial variations in the physical and elastic properties of subsurface materials (Chen et al., 2023; Lacombe et al., 2023; Sibson, 2020; Zhao et al., 2025). Processes such as fault displacement, fracturing, weathering, hydrothermal alteration, and fluid circulation progressively modify the mechanical behavior of rocks, resulting in pronounced lateral and vertical heterogeneity in density, stiffness, and seismic impedance (Bedford et al., 2022; Song et al., 2024). These heterogeneous conditions strongly influence seismic-wave propagation, control the distribution of shear-wave velocities, and govern the spatial variability of ground response (de la Torre et al., 2022; Huang et al., 2019). Consequently, characterizing subsurface elastic heterogeneity has become an important component of tectonic investigations because it provides valuable insights into fault architecture, deformation mechanisms, and seismic hazards.

In normal fault environments, long-term extensional deformation produces fault cores and surrounding damage zones that commonly consist of fractured and weathered materials with reduced rigidity relative to the adjacent host rocks (Lacombe et al., 2023; Pischiutta et al., 2012). Such deformation modifies the geometry of subsurface layers and generates localized velocity contrasts over relatively short distances (Weydt et al., 2022). These mechanical discontinuities are often difficult to recognize through surface geological observations alone, particularly where deformation is obscured by young sedimentary deposits or hydrothermal alteration (Elfadly et al., 2026). Therefore, geophysical investigations capable of resolving spatial variations in subsurface elastic properties provide an effective means of examining the internal structure of fault zones and improving geological interpretations beyond surface mapping (Li et al., 2025).

Ambient vibration measurements using the Horizontal-to-Vertical Spectral Ratio (HVSR) method have become one of the most widely adopted passive geophysical techniques for investigating shallow subsurface conditions (Galone et al., 2026; Vergara-huerta and Aguirre, 2020). Numerous studies have demonstrated the capability of HVSR to estimate fundamental resonance frequency, impedance contrast, sediment thickness, site amplification, and seismic vulnerability in both sedimentary basins and tectonically active regions (Perez, 2024; Silahtar et al., 2026; Stanko and Markušić, 2020). The development of HVSR inversion techniques has further expanded these applications by enabling the reconstruction of one-dimensional shear-wave velocity (Vs) models that provide quantitative information on subsurface elastic properties (Molnar et al., 2022; Olivares-palomares et al., 2025). More recently, several studies have combined HVSR-derived velocity models with geological, geotechnical, and geophysical observations to investigate lithological variations, sedimentary basin architecture,

and fault-controlled subsurface structures, demonstrating that ambient vibration measurements can contribute to broader geological interpretations beyond conventional site-response assessments (Cherki et al., 2026; Kang et al., 2020; Tarabusi et al., 2024).

Previous studies demonstrate that HVSR and its inversion can constrain near-surface velocity structure; however, the extent to which spatially variable velocity patterns can be distinguished from lithological or fault-related effects remains site dependent. In many fault-related investigations, spatial variations in shear-wave velocity are commonly interpreted as consequences of changes in lithology or weathering intensity, whereas their relationships with localized deformation, fault damage zones, and internal structural architecture receive comparatively less attention (Medwedeff et al., 2021). Furthermore, while HVSR inversion has become increasingly common, most interpretations remain based on individual one-dimensional velocity profiles, limiting the ability to evaluate the spatial continuity of subsurface heterogeneity across fault systems (Gosselin et al., 2022; Mianshui et al., 2022; Zaenudin et al., 2022; Zhu et al., 2020). Consequently, the extent to which velocity discontinuities and localized low-velocity anomalies reflect fault-related deformation, subsidiary fault development, or concealed structural complexity remains insufficiently constrained in many tectonically active environments.

The Palolo Fault, one of the active normal fault segments associated with the Palu–Koro Fault System in Central Sulawesi, Indonesia (Patria et al., 2026a; Patria and Putra, 2020), represents an appropriate natural laboratory for investigating these issues. This fault has experienced prolonged tectonic deformation that has influenced the regional geological framework and contributed to the development of complex lithological contacts, hydrothermal manifestations, and heterogeneous subsurface conditions (Bedford et al., 2022; Duwiquet et al., 2021; Elfadly et al., 2026; Serhalawan and Chen, 2024). Despite its tectonic significance, the spatial distribution of subsurface elastic properties across the fault zone and their relationship to fault-related deformation remain poorly understood. Improved characterization of these properties is therefore essential for understanding the internal architecture of the fault zone and evaluating the geological processes responsible for its present-day structural complexity.

In this study, ambient vibration measurements are integrated with HVSR inversion to investigate subsurface heterogeneity across the Palolo Fault in the Bora geothermal area, Central Sulawesi. Instead of limiting the interpretation to conventional site-response parameters, the inverted shear-wave velocity models are synthesized into continuous two-dimensional subsurface sections to evaluate the spatial distribution of velocity contrasts, localized low-velocity zones, and structural discontinuities associated with fault-related deformation. The

resulting velocity models provide additional constraints on subsurface heterogeneity around the Palolo Fault and may indicate possible concealed fault-related structures that are not readily recognized from surface geological observations alone. The combined analysis provides additional information on the spatial organization of near-surface elastic heterogeneity around the Palolo Fault and demonstrate the broader potential of HVSR-derived shear-wave velocity models for investigating structural complexity within active tectonic environments.

2 Geological and Tectonic Setting

Central Sulawesi is one of the most tectonically active regions in Indonesia and has experienced prolonged crustal deformation associated with the interaction of several tectonic blocks (Patria et al., 2026b; Purba et al., 2026). These tectonic processes have controlled the development of geological structures, sedimentary basins, and hydrothermal systems, giving rise to a complex geological framework throughout the region (Tawil, 2024).

The study area is located in Sigi Biromaru District, Sigi Regency, Central Sulawesi Province, Indonesia (Fig. 1) within the tectonic domain influenced by the Palolo Fault, one of the active fault segments associated with the Palu-Koro Fault System in Central Sulawesi. According to the Indonesian National Earthquake Source and Hazard Center (PUSGEN)(PuSGeN, 2025), the Palolo Fault trends predominantly northwest-southeast and represents an important normal fault that has played a significant role in the geological evolution of the surrounding region (Frando et al., 2025; Nuarta et al., 2024). Prolonged tectonic activity along this fault has contributed to the present-day structural framework and influenced the distribution of geological units across the study area (Aditama et al., 2025; Rosid et al., 2023).

The Gumbasa Complex mainly consists of metamorphic rocks, including schist, gneiss, quartzite which generally exhibit high competence and relatively high seismic velocities (Nuarta et al., 2024; Rohit et al., 2021). In contrast, the Quaternary alluvial deposits are composed of unconsolidated materials such as sand, gravel, silt, and clay, which are characterized by lower rigidity and lower shear-wave velocities (Silahtar et al., 2025). Consequently, the coexistence of these lithological units is expected to produce significant impedance contrasts and lateral variations in elastic properties beneath the study area.

The coexistence of contrasting lithological units and the prolonged tectonic evolution associated with the Palolo Fault have produced a complex geological framework within the study area (Janssens, 2024). Variations in lithology, degree of consolidation, and weathering intensity are expected to generate significant contrasts in physical and elastic properties, resulting in pronounced lateral and vertical heterogeneity beneath the surface.

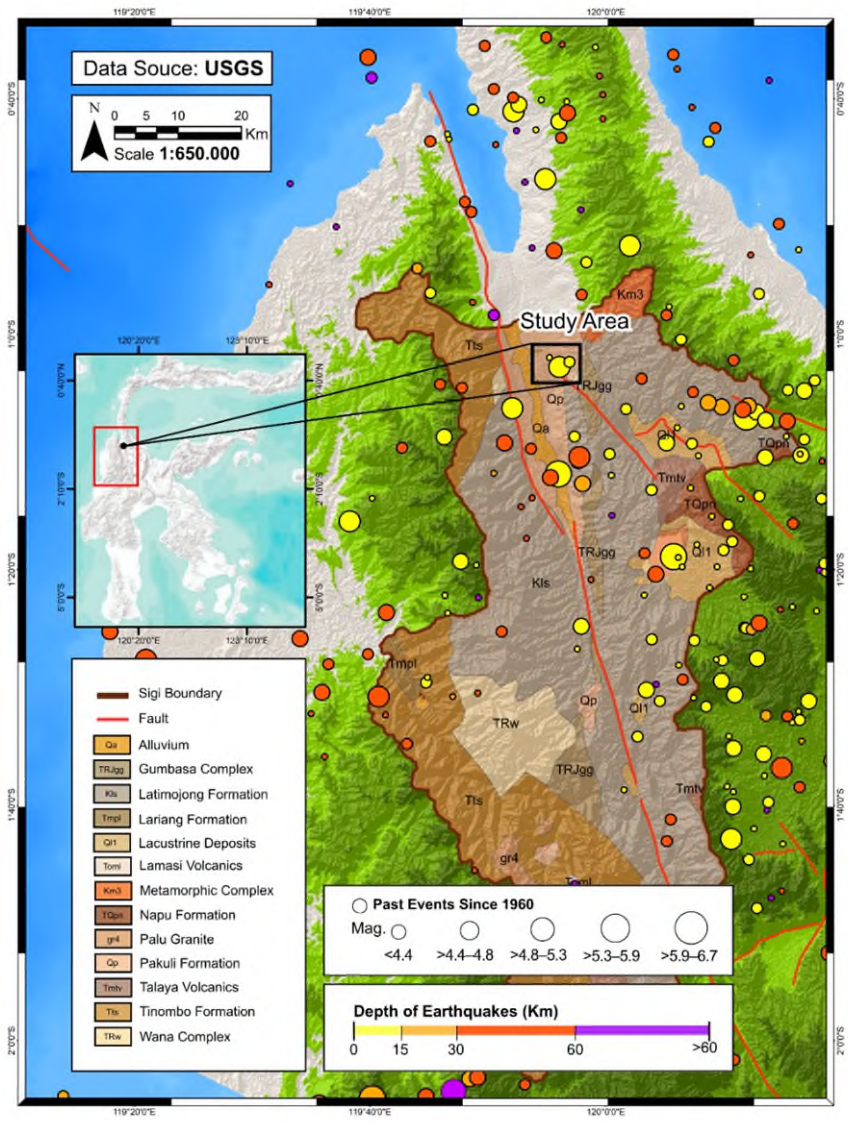


Fig. 1 Geological and seismicity map of the study area in Central Sulawesi, Indonesia. Historical earthquakes recorded since 1960 from the United States Geological Survey (USGS) earthquake catalog are shown as colored circles, where the circle color represents focal depth and the circle size corresponds to earthquake magnitude. The Palolo Fault is represented by the red line, and the black rectangle marks the HVSR survey area. The geological map shows the distribution of the major lithological units. The inset map indicates the location of the study area within Central Sulawesi, Indonesia

3 Methodology

3.1 Ambient Vibration Measurements

Ambient vibration measurements were conducted in Sigi Biromaru District, Sigi Regency, Central Sulawesi, Indonesia, which is located in the vicinity of the Palolo Fault. A total of 25 measurement points was distributed along two survey lines, Line A and Line B, as illustrated in Fig. 2. The survey geometry was designed to traverse the inferred structural trend in order to facilitate the observation of lateral variations in subsurface elastic properties across the fault zone.

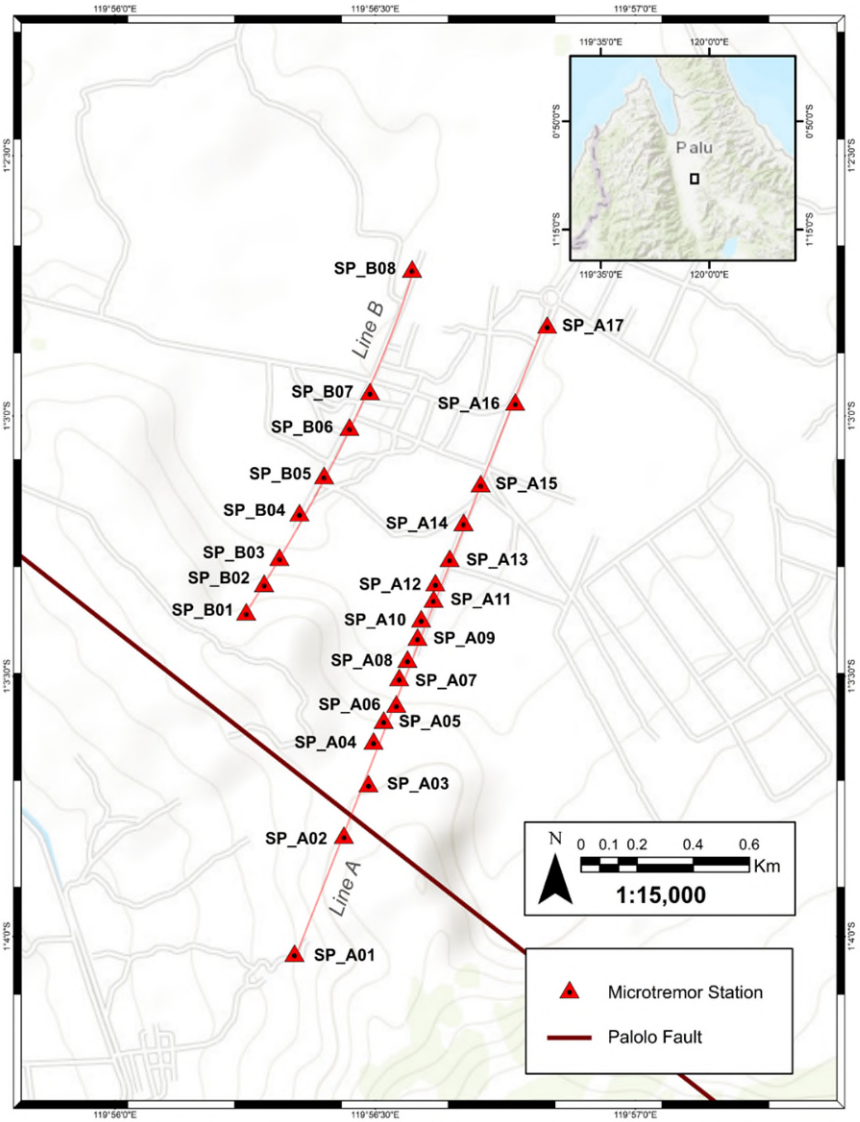


Fig. 2 Location map of ambient vibration measurement stations in the Bora area, Sigi Regency, Central Sulawesi, Indonesia. 25 ambient vibration stations (red triangles) were distributed along two survey lines across the study area, while the red line represents the mapped trace of the Palolo Fault based on PUSGEN data. The inset map indicates the geographical location of the study area within Central Sulawesi. The survey configuration was designed to investigate lateral variations in subsurface properties and their relationship with the Palolo Fault zone

Microtremor recordings were acquired using a three-component MBB-2, which simultaneously records the north–south (NS), east–west (EW), and vertical (UD) components. Each station was recorded for 60 min with a sampling frequency of 100 Hz. The relatively long recording duration was adopted to ensure sufficient ambient vibration cycles at low frequencies and to improve the stability of spectral estimates. The data processing workflow is illustrated in Fig. 3.

To minimize the influence of anthropogenic noise, the sensors were installed on relatively flat ground and placed as far as possible from local disturbance sources. In addition, sensor orientations were carefully maintained

along the north–south and east–west directions to ensure that the recorded three-component signals accurately represented the subsurface conditions.

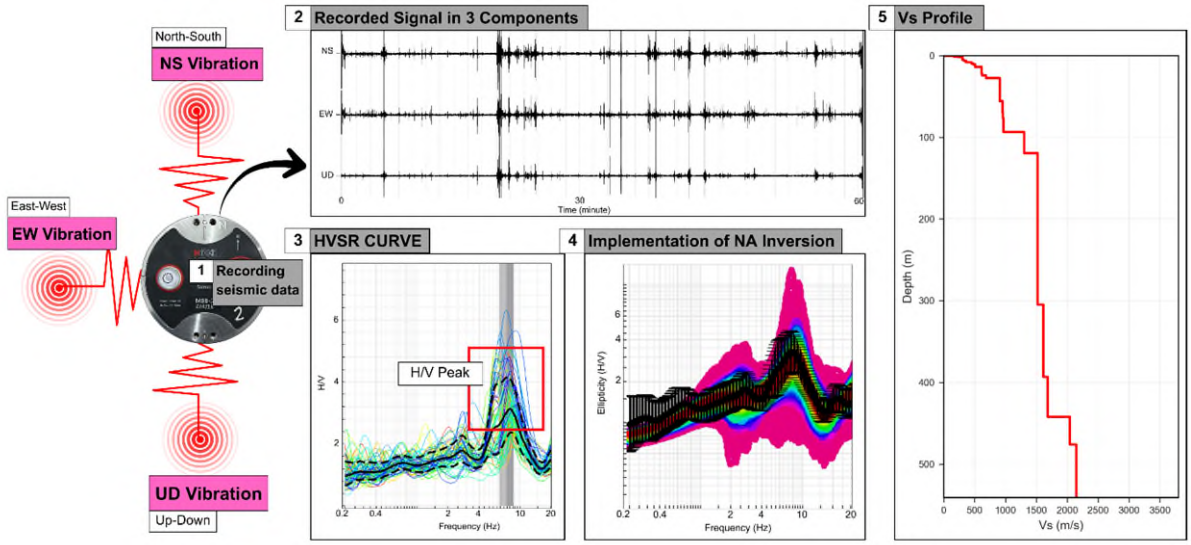


Fig. 3 Workflow of the Horizontal-to-Vertical Spectral Ratio (HVSR) data processing used to obtain the shear-wave velocity (Vs) profile. The procedure begins with (1) the acquisition of ambient vibration (microtremor) data using a three-component seismometer (North–South, East–West, and Up–Down). (2) the recorded signals from the three components are displayed in the time domain. (3) HVSR curve analysis is performed to determine the dominant frequency (f_0) and peak amplitude (A_0) based on the H/V spectral peak. The resulting HVSR curve is then used as the input for (4) nonlinear inversion using the Neighborhood Algorithm (NA) to obtain the shear-wave velocity model that best fits the observed data. (5) a one-dimensional shear-wave velocity (Vs) profile with depth is generated, representing the subsurface structure

3.2 HVSR Analysis and Site Response Parameters

Microtremor data were processed using the HVSR technique. Time-series records were first divided into 60-s windows to select stationary segments and reduce the effects of transient noise. Stable windows were subsequently transformed into the frequency domain using the Fast Fourier Transform (FFT).

The HVSR curve was calculated as the ratio between the horizontal and vertical spectral amplitudes according to Eq (1) (Meng et al., 2023):

$$HVSR(f) = \sqrt{\frac{H_{NS}{}^2(f)+H_{EW}{}^2(f)}{2V^2(f)}}, \quad (1)$$

where $H_{NS}(f)$ and $H_{EW}(f)$ denote the Fourier spectra of the north–south and east–west horizontal components, respectively, while $V(f)$ represents the spectrum of the vertical component.

To obtain smoother and more stable spectral curves, Konno–Ohmachi smoothing with a bandwidth coefficient of 50 was applied (Nardone et al., 2020; Perez, 2024; Zhu et al., 2020). The resulting HVSR curves provided two principal parameters, fundamental frequency and peak (f_0) amplification (A_0) which reflect the

impedance contrast and resonance characteristics of the subsurface (Akin et al., 2026; Rigo et al., 2021; Silahtar et al., 2026; Stanko and Markušić, 2020).

These parameters were subsequently used to calculate vulnerability index Kg proposed by Nakamura was calculated as Eq (2) (Nakamura, 2000):

$$K_g = \frac{A_0{}^2}{f_0} \quad , (2)$$

where Kg is the seismic vulnerability index calculated from A_0 and f_0. Higher Kg values are interpreted here as larger HVSR-based vulnerability-index values. A_0 denotes the peak amplification of the HVSR response, while f_0 corresponds to the fundamental frequency associated with the resonance characteristics of the subsurface.

3.3 HVSR Inversion and Shear Wave Velocity Modelling

HVSR inversion was performed using the Dinver module implemented in Geopsy based on the Neighborhood Algorithm (NA). This global optimization approach employs a Monte Carlo search strategy to efficiently explore the parameter space and avoid convergence to local minima (Ai et al., 2026; Barone et al., 2021; Keil and Wassermann, 2023; Nagamani et al., 2020; Provenzano and Ludovic, 2025; Vantassel and Cox, 2021). Each trial model consisted of layer thickness (h), shear-wave velocity (Vs), compressional-wave velocity (Vp), and density (ρ).

The subsurface was parameterized as a 24-layer model overlying a half-space in Table 1. These parameter bounds constrained the inversion while allowing sufficient flexibility to reproduce the observed HVSR curves and were selected because they govern the elastic behavior and impedance contrasts of subsurface materials, which strongly influence the resonance characteristics and shape of the HVSR curve. Parameter ranges were defined based on reasonable geological and geophysical constraints to ensure physically meaningful solutions during the inversion process.

These parameters were used to evaluate lateral variations in subsurface elastic properties and served as constraints for the inversion process to derive shear-wave velocity models. For each trial model, synthetic HVSR curves were generated and compared with the observed curves. Models with smaller misfit values were considered to provide better agreement and were subsequently used as the basis for further parameter exploration (Gupta et al., 2021; Kong et al., 2021; Nagamani et al., 2020; Olafsdottir and Erlingsson, 2020; Rahimi et al., 2021; Seivane et al., 2022; Winkens et al., 2026). This iterative approach progressively reduced the parameter space toward regions containing optimal solutions (Ai et al., 2026; Zaenudin et al., 2022). In contrast to local optimization techniques, the Neighborhood Algorithm allows multiple acceptable solutions to be obtained, thereby providing a better

assessment of model uncertainty (Dabhi and Pandya, 2020; Juan et al., 2021; Panadero et al., 2018; Zhang et al., 2019).

Table 1. Parameter ranges adopted for the HVSR inversion. The subsurface was represented by a 24-layer model overlying a half-space corresponding to the seismic bedrock. The inversion parameters include layer depth, compressional-wave velocity (Vp), shear-wave velocity (Vs), and density ranges used to constrain the search space during the Neighborhood Algorithm optimization

Layers	**Depth (m)**	**Vp (m/s)**	**Vs (m/s)**	**ρ (kg/m3)**
L1	1-2	257-1000	90-500	1800-2100
L2	2-3	257-1200	90-630	1800-2100
L3	1-5	257-1500	90-735	1685-1885
L4	1-7	257-1900	90-815	1773-1973
L5	2-11	257-2200	90-880	1832-2032
L6	3-17	257-2416	90-935	1871-2071
L7	5-26	257-2467	90-975	1880-2080
L8	7-38	257-2517	90-1010	1888-2088
L9	10-54	261-2567	96-1040	1897-2097
L10	13-72	273-2609	112-1065	1906-2106
L11	18-95	295-2634	135-1080	1914-2114
L12	23-121	327-2659	163-1095	1923-2123
L13	26-138	384-2693	203-1115	1938-2138
L14	39-201	470-2844	252-1205	1974-2174
L15	50-251	606-3054	316-1330	2024-2224
L16	58-300	797-3306	392-1480	2082-2282
L17	70-361	1037-3628	477-1675	2150-2350
L18	84-429	1328-3984	572-1895	2221-2421
L19	100-503	1635-4381	670-2150	2291-2491
L20	115-585	1926-4774	766-2420	2354-2554
L21	133-674	2175-5140	855-2695	2406-2606
L22	154-774	2351-5446	927-2955	2445-2645
L23	176-883	2458-5679	978-3185	2471-2671
L24	200-1000	2494-5822	997-3350	2485-2685
Half Space	-	6000	3500	2700

The agreement between observed and synthetic HVSR curves were evaluated using misfit, expressed as Eq (3) (Rosalia et al., 2022):

$$\text{misfit} = \sqrt{\sum_{i=0}^{n} \frac{HV_{di}(f_i) - HV_{ci}(f_i)}{\sigma_{i_{HV}}(f_i)}}, \quad (3)$$

where HV_{di} and HV_{ci} represent the observed and calculated ellipticity values at frequency f_i, respectively, and $\sigma_{i_{HV}}$ denotes the associated uncertainty.

Models with misfit values <1 were selected as representative solutions because they provided satisfactory agreement with the measured HVSR curves (Avila, V et al., 2025; Krylov et al., 2022; Rosalia et al., 2022; Stanko and Markušić, 2020). Model selection was based not only on the minimum misfit value but also on the stability of the curve shape and the consistency among low-misfit solutions (Fichtner et al., 2021; Gosselin et al., 2022; Laby et al., 2025).

The inverted shear-wave velocity models were used to investigate the distribution of subsurface elastic properties and their relationship to fault-related deformation. Active fault zones are commonly characterized by fractured and weathered materials that exhibit reduced rigidity and consequently lower shear-wave velocities than the surrounding rocks (Abdelrahman, 2025; Abdelrahman et al., 2024; Shu and Li, 2026). Such conditions may generate significant velocity contrasts and structural discontinuities within the subsurface (Kim et al., 2026; Mi et al., 2020; Scarponi et al., 2024; Tan et al., 2026; Tang et al., 2022). Localized low-velocity zones and abrupt lateral variations in Vs over relatively short distances may indicate deformation zones, lithological boundaries, or concealed fault-related structures (Caputo et al., 2026; Feng et al., 2026).

3.4 Two-Dimensional Shear-Wave Velocity Modeling

Two-dimensional shear-wave velocity models obtained from HVSR inversion at individual measurement sites were integrated to construct two-dimensional (Vs) sections along Lines A and B. This approach was intended to visualize the lateral and vertical distribution of elastic properties and to identify structural discontinuities potentially associated with fault-related deformation.

Each inverted Vs model was assigned according to its actual measurement location, and the velocity distribution with depth at each station was used as input for constructing continuous two-dimensional models. Spatial interpolation between neighboring stations was performed using the Ordinary Kriging method. Ordinary Kriging was used to interpolate the station-based Vs estimates onto a regular grid while accounting for spatial covariance among neighboring observations. The resulting sections should be regarded as interpolated representations between measurement points. (Boumpoulis et al., 2023).

The resulting two-dimensional sections were used to evaluate lateral variations in shear-wave velocity, changes in the thickness of low-velocity layers, and the geometry of subsurface structures (Abdelrahman and Alarifi, 2026; Zhang et al., 2025). Low Vs zones generally represent fractured, weathered, or hydrothermally altered materials characterized by lower rigidity, whereas high Vs regions correspond to more competent and less deformed rocks (Pereira et al., 2026).

In faulted environments, abrupt lateral changes in Vs localized low-velocity anomalies, and rapid variations in layer geometry may reflect fault cores, deformation zones, or previously unrecognized may indicate the presence of a fault due to the Vs contrast anomaly (Bruno et al., 2025). Therefore, two-dimensional shear-wave velocity models provide important constraints for investigating subsurface heterogeneity and structural complexity across the Palolo Fault zone.

4 Results

4.1 Characteristics of HVSR Parameters

Microtremor analysis using the Horizontal-to-Vertical Spectral Ratio (HVSR) method at 25 measurement stations distributed along Lines A and B reveals significant lateral variations in subsurface dynamic response characteristics. These variations are clearly reflected in the HVSR curves shown in Fig. 4 and Fig. 5, which exhibit differences in dominant frequency (f_0), peak amplitude (A_0), and spectral complexity among measurement points.

The HVSR curves along Lines A and B exhibit two principal characteristics, low-frequency and high-frequency dominant responses. Low dominant frequencies are commonly associated with thicker or softer near-surface layers, whereas higher frequencies may occur where the resonant layer is shallower or stiffer, producing resonance at lower frequencies due to strong impedance contrasts between soft sediments and underlying stiffer materials. In contrast, high dominant frequencies suggest thinner sedimentary cover or rapid lateral changes in subsurface properties over short distances. These observations are consistent with the findings of Kang et al. (2020), who reported that low dominant frequencies correlate with greater sediment thickness, whereas high dominant frequencies are associated with shallow sediments or shallow bedrock. Furthermore, according to the SESAME (2004), clear and stable HVSR peaks provide reliable indicators of local resonance frequency and subsurface impedance contrast.

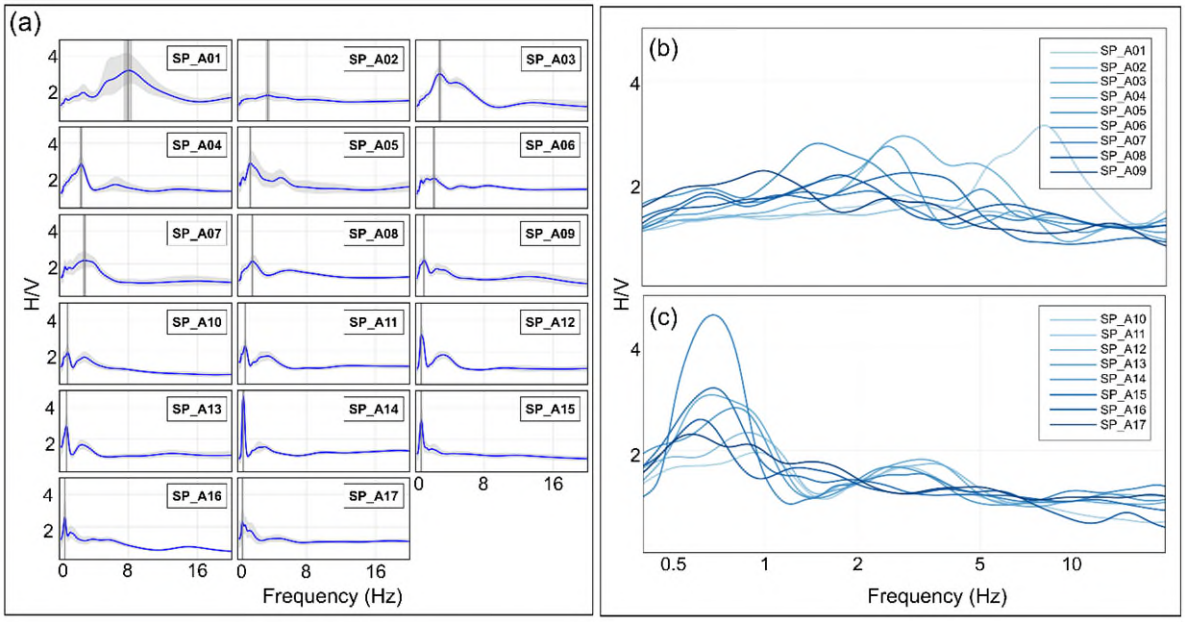


Fig. 4 HVSR curves for all measurement stations along Line A. (a) Individual HVSR curves for each measurement station along Line A, the solid blue lines represent the average HVSR curves, gray shaded areas indicate standard deviation, and vertical gray lines mark the dominant frequency peaks, (b) HVSR curves showing high-frequency dominant responses (0.90-7.54 Hz) for stations SP_A01 to SP_A09. (c) HVSR curves showing low-frequency dominant responses (0.57 to 0.84 Hz) for stations SP_A10 to SP_A17. These curves illustrate variations in dominant frequency and peak amplitude across Line A

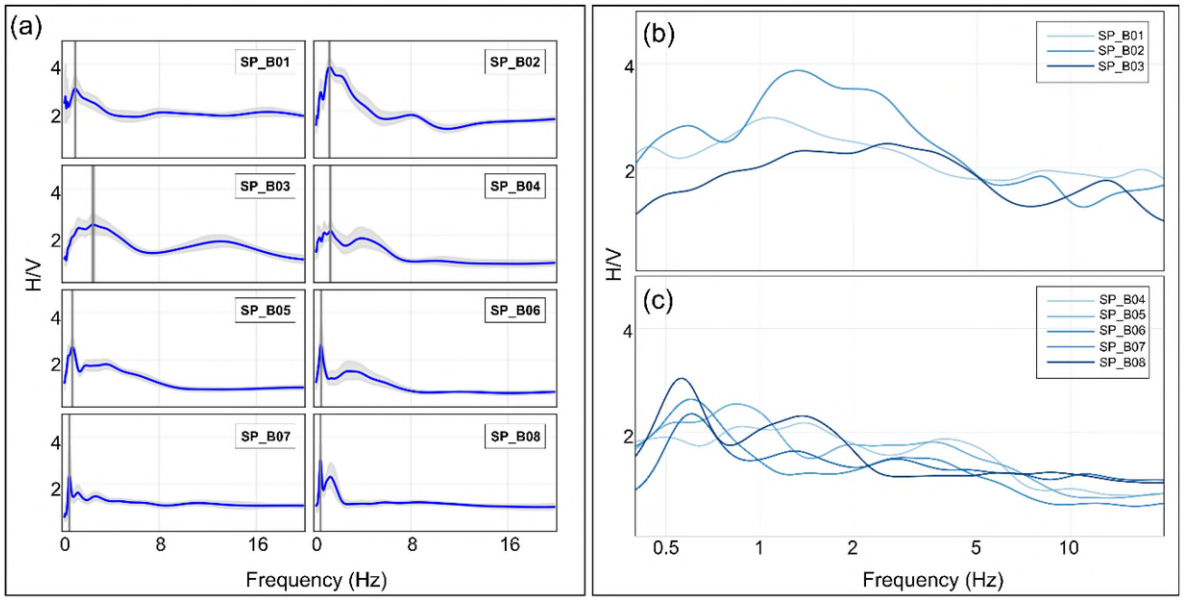


Fig. 5 HVSR curves for all measurement stations along Line B. (a) Individual HVSR curves for each measurement station along Line B, the solid blue lines represent the average HVSR curves, gray shaded areas indicate standard deviation, and vertical gray lines mark the dominant frequency peaks, (b) HVSR curves showing high-frequency dominant responses (1.07-2.62 Hz) for stations SP_B01 to SP_B03, (c) HVSR curves showing low-frequency dominant responses (0.55-0.82 Hz) for stations SP_B04 to SP_B08. These curves illustrate variations in dominant frequency and peak amplitude across Line B

The spatial distribution of resonance response in the HVSR pseudosection (Fig. 6) reveals contrasting patterns between the two measurement lines. Along Line A, dominant responses are mainly concentrated within low to intermediate frequency ranges, with a pronounced anomaly observed around stations SP_A11 to SP_A15, characterized by high normalized amplitudes. This anomaly suggests lateral variations in subsurface structure, likely associated with changes in impedance contrast or localized geological structures. In contrast, Line B exhibits dominant responses at relatively higher frequencies, particularly around SP_B01 to SP_B02. The contrasting resonance patterns between the two lines indicate significant lateral heterogeneity in subsurface conditions. According to Syamsuddin et al. (2026) lateral changes in H/V amplitude patterns within pseudosections commonly reflect shallow geological heterogeneity, including lithological variation, sediment thickness changes, and subsurface discontinuities.

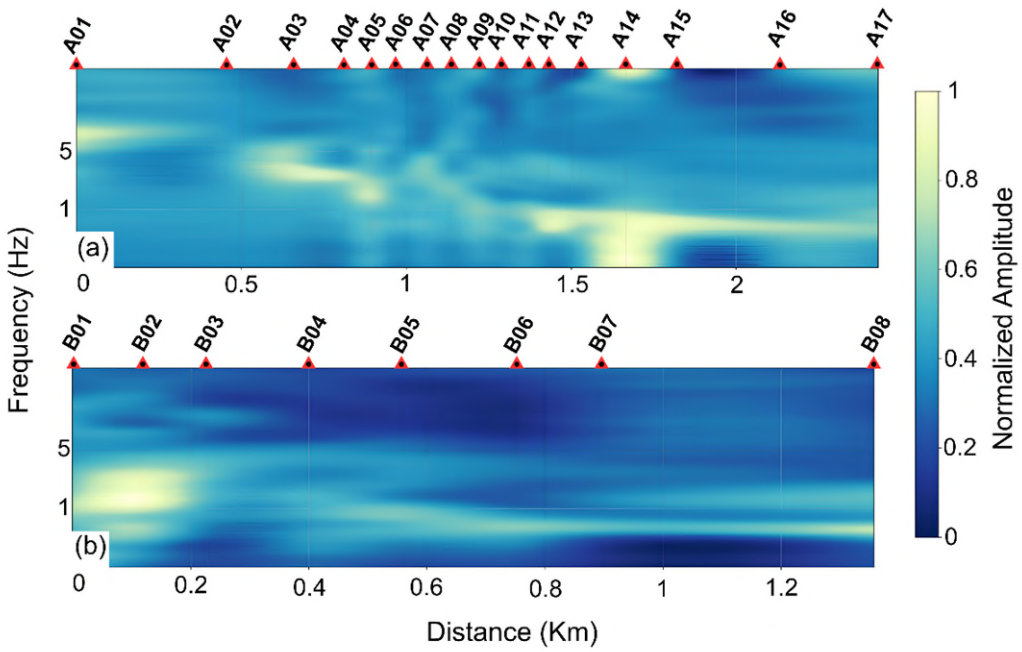


Fig. 6 HVSR pseudosections along Lines A and B showing the spatial distribution of normalized H/V amplitude. The horizontal axis represents distance along each measurement line, while the vertical axis represents frequency (Hz). Red triangles indicate microtremor measurement stations. Colors represent normalized H/V amplitudes, ranging from dark blue (low amplitude) to yellow (high amplitude). High-amplitude zones indicate stronger resonance responses and potential subsurface impedance contrasts

The station-based distribution of HVSR parameters shown in Fig. 7 further highlights variations in subsurface dynamic characteristics at individual measurement points. The bar-chart representation clearly shows fluctuations in f_0, A_0, and Kg values between adjacent stations along both lines, indicating rapid lateral changes in subsurface physical properties. Several stations along Line A, particularly SP_A11 to SP_A15, exhibit relatively Stations SP_A11-SP_A15 show relatively low f0 and elevated Kg values, indicating a distinct low-frequency HVSR response. Along Line B, station SP_B04 also shows relatively low f_0 and elevated Kg compared to neighboring stations. These local anomalies indicate zones with distinct mechanical contrasts and potentially significant subsurface heterogeneity.

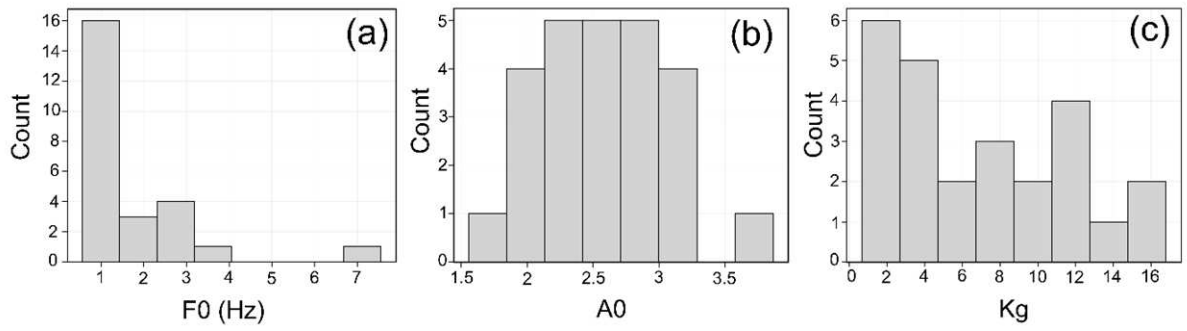


Fig. 7 Station-based distribution of HVSR parameters for all measurement points along Lines A and B. Bar charts represent the values of dominant frequency (f0), peak amplitude (A0), and seismic vulnerability index (Kg) for each measurement station

The spatial distribution of HVSR parameters derived from interpolation (Fig. 8) further confirms significant subsurface heterogeneity across the study area. The dominant frequency (f_0) generally decreases from south to north, indicating progressively thicker sediment accumulation toward the northern part of the study area (Fig. 8a). Stations with A0 > 2 show relatively stronger H/V peak amplitudes, which may reflect stronger impedance contrasts within the resonant structure between sedimentary layers and underlying stiffer materials, whereas low A0 values (<2) suggest relatively homogeneous subsurface conditions (Fig. 8b). The Kg distribution identifies zones with higher Kg values, particularly around SP_A11-SP_A15, indicating stronger values of the adopted HVSR-based vulnerability index, characterized by low f_0 and high Kg values (Fig. 8c). Notably, several HVSR anomalies spatially coincide with or occur near the mapped trace of the Palolo Fault Segment B, suggesting that regional tectonic structures may influence local subsurface heterogeneity and dynamic site response. These findings are consistent with Rahayu et al., (2022) who reported that the combination of low f_0, high A_0, and high Kg commonly indicates zones of greater seismic vulnerability associated with thick soft sediments and strong impedance contrasts.

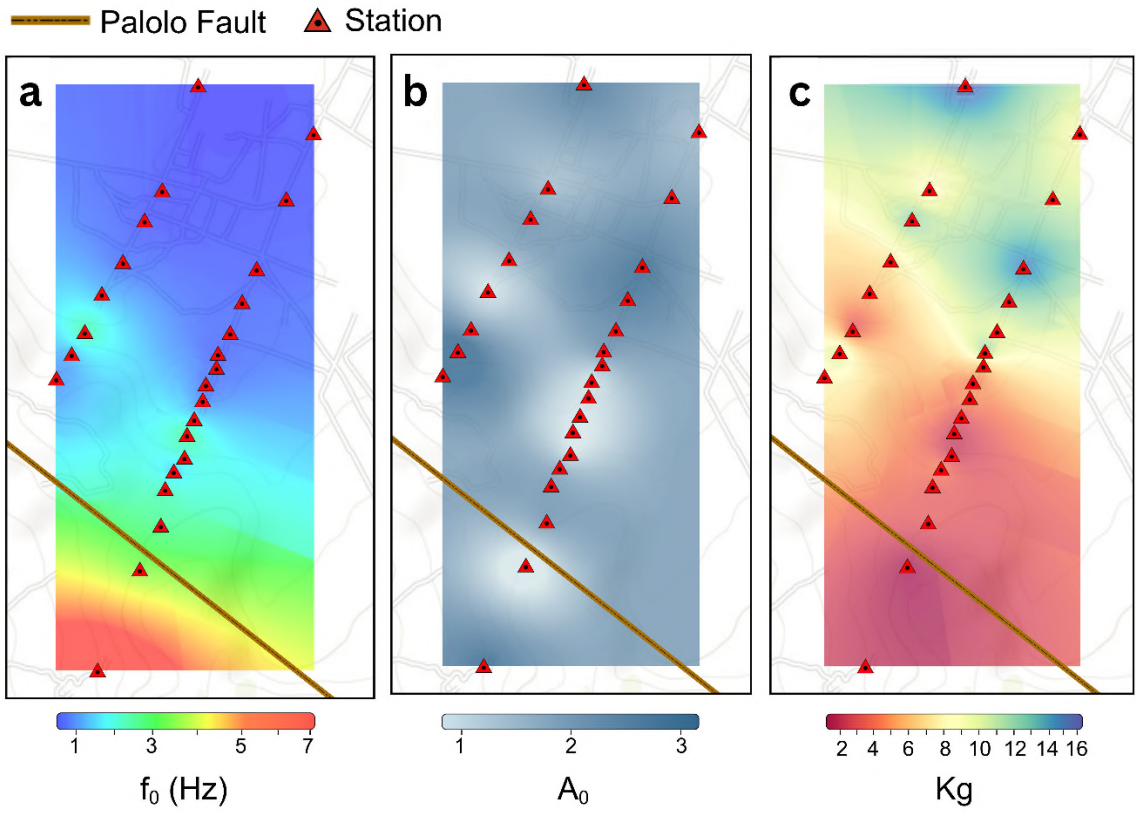


Fig. 8 Spatial distribution of HVSR parameters derived from ordinary Kriging interpolation across the study area. (a) Spatial distribution of dominant frequency (f0), with colors ranging from blue (low frequency) to red (high frequency), representing variations in sediment thickness and subsurface stiffness, (b) Spatial distribution of peak amplitude (A0), with colors ranging from white (low amplitude) to blue (high amplitude), (c) Spatial distribution of seismic vulnerability index (Kg), with colors ranging from dark red (low vulnerability) to dark green (high vulnerability)

4.2 Shear-Wave Velocity from HVSR Inversion

To obtain a more quantitative characterization of the subsurface structure, the HVSR curves at each measurement station were inverted into shear-wave velocity (Vs) models. The inversion results provide constraints on the elastic properties of subsurface materials and allow differentiation between soft sediments, weathered layers, and more competent bedrock. The consistency of the inversion results was first evaluated from the misfit between observed and modeled HVSR curves, which quantify the agreement between observed and modeled HVSR curves. As shown in Fig. 9, all stations exhibit relatively low misfit values, ranging from approximately 0.03 to 0.08, indicating a satisfactory agreement between the observed data and inversion results.

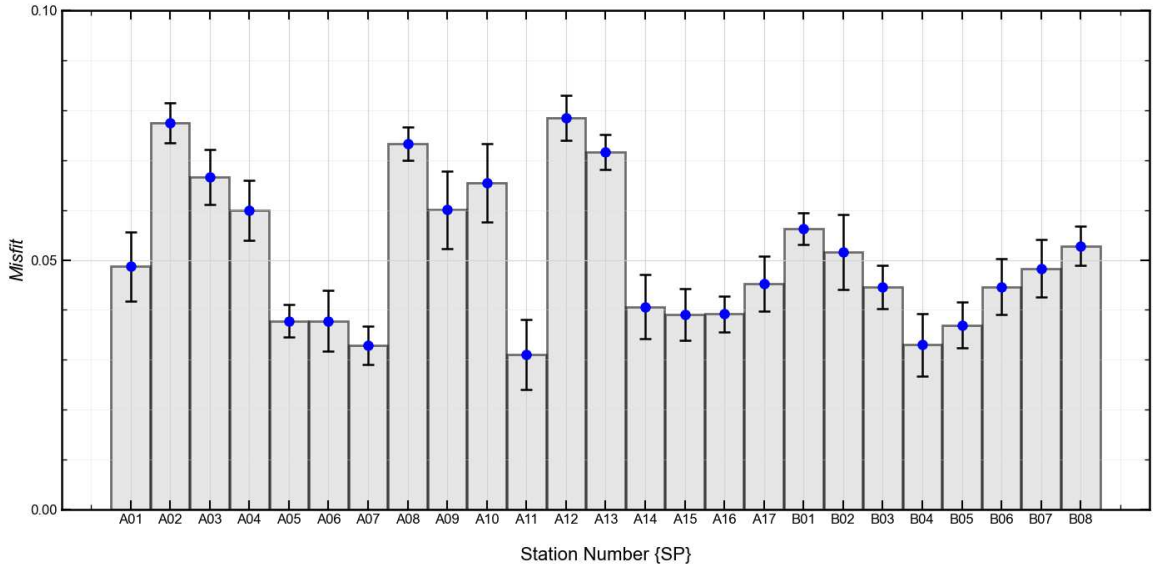


Fig. 9 Distribution of misfit values obtained from HVSR inversion for all measurement stations. Bar plots represent the misfit values calculated for each measurement station. Low misfit values indicate good agreement between observed HVSR responses and inversion-derived theoretical models. Stations with lower misfit values are considered to provide more reliable subsurface velocity models for further interpretation

In addition to quantitative evaluation through misfit values, inversion quality was further validated by comparing observed HVSR curves with theoretical responses generated from accepted inversion models at representative stations along Lines A and B (Fig. 10 and Fig. 11). Overall, the theoretical curves successfully reproduce the main characteristics of the observed HVSR responses, particularly the dominant resonance peaks, spectral shapes, and peak amplitudes. The strong correspondence between observed and theoretical responses indicates that the inversion models effectively capture the principal impedance contrasts controlling local site response. A long Line A, several stations display sharp low-frequency resonance peaks, reflecting strong impedance contrasts between near-surface sediments and deeper stiff layers. Along Line B, the theoretical curves also show good agreement with observed responses, although minor amplitude deviations are observed at several stations, likely due to local heterogeneity or environmental noise. Similar observations were reported by Rong et

al. (2021), who emphasized that a close match between observed and theoretical HVSR curves is a key indicator of inversion reliability.

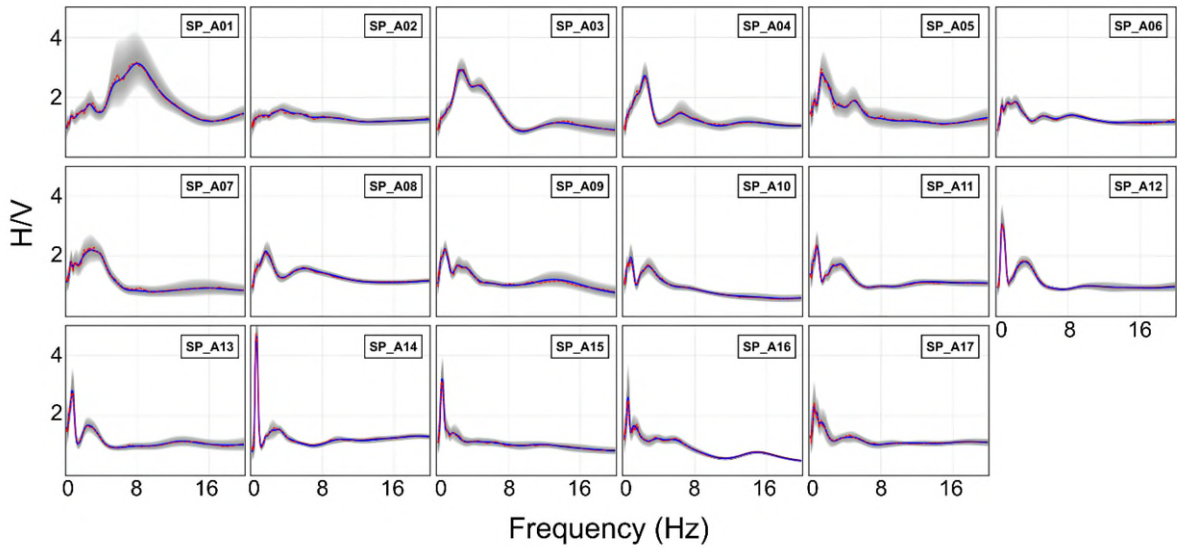


Fig. 10 Comparison of observed and theoretical HVSR curves at selected representative stations along Line A. Solid blue lines represent observed HVSR responses, while dashed red lines represent theoretical responses calculated from accepted inversion models. Gray shaded areas indicate uncertainty ranges of observed HVSR data. The overall agreement between the two curves demonstrates that the inversion-derived subsurface models adequately reproduce the main resonance characteristics and impedance contrasts controlling site response

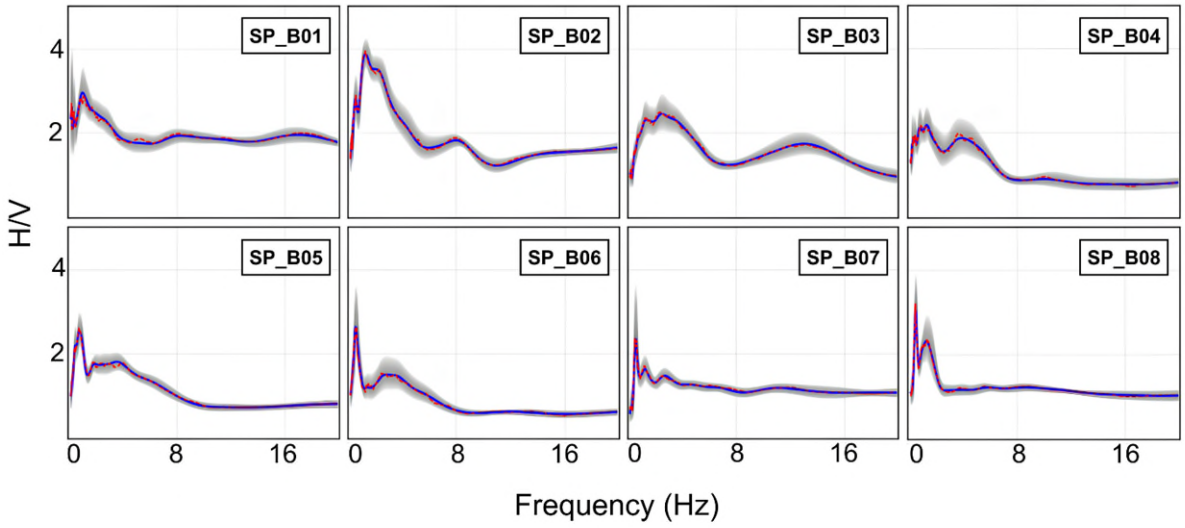


Fig. 11 Comparison of observed and theoretical HVSR curves at selected representative stations along Line B. Solid blue lines represent observed HVSR responses, while dashed red lines represent theoretical responses calculated from accepted inversion models. Gray shaded areas indicate uncertainty ranges of observed HVSR data. The close correspondence between observed and theoretical responses indicates that the inversion models reliably capture the main resonance features of the subsurface

The one-dimensional shear-wave velocity profiles for all stations along Lines A and B are presented in Fig. 12. The inversion results show a general increase in Vs with depth, reflecting the transition from unconsolidated near-surface sediments to progressively more compact and mechanically competent materials.

Near-surface layers are generally characterized by low Vs values (<500 m/s), corresponding to lose sediments or soft soil deposits with low compaction. Intermediate layers commonly exhibit Vs values ranging from 500 to 1500 m/s, representing compacted sediments or weathered rock. At greater depths, Vs values exceed 1500 m/s, indicating stiff materials or bedrock. This progressive increase in velocity with depth is consistent with the general behavior of sedimentary environments, where increasing density and stiffness produce higher seismic-wave velocities (Yulianur et al., 2020).

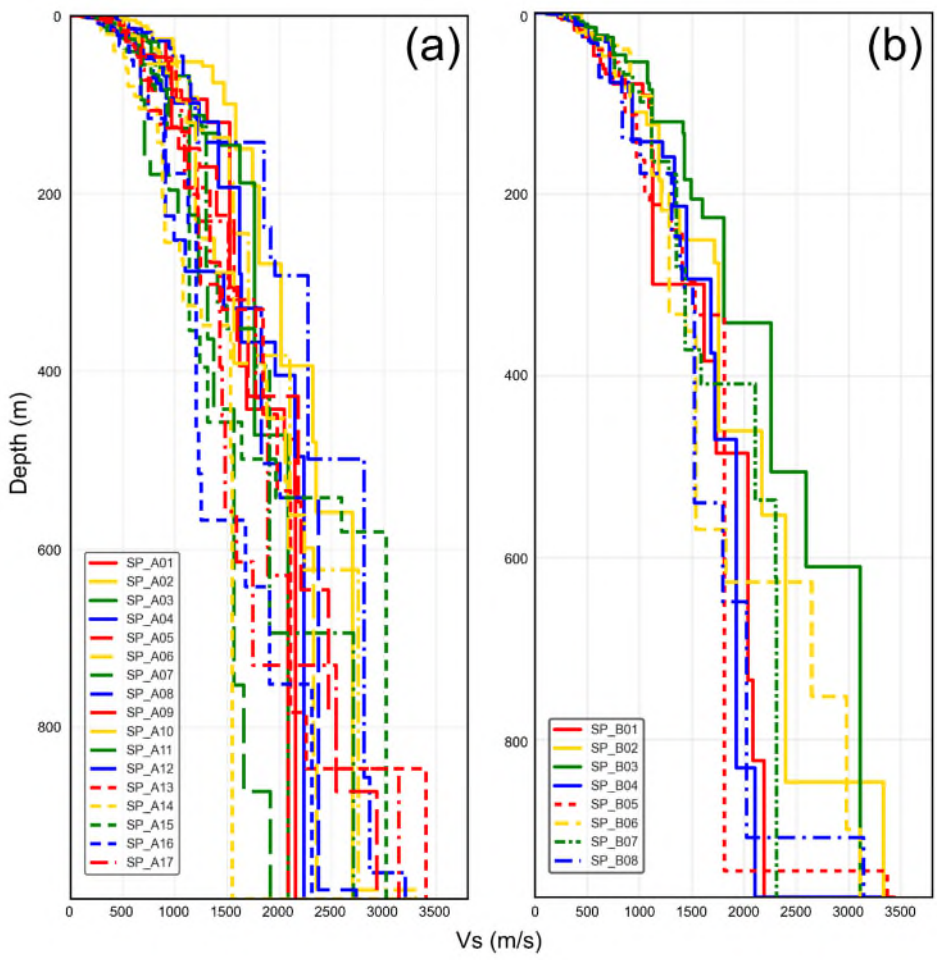


Fig. 12 One-dimensional shear-wave velocity (Vs) profiles derived from HVSR inversion. (a) Line A (SP_A01–SP_A17), (b) Line B (SP_B01–SP_B08). Horizontal axis shows Vs (m/s), and vertical axis shows depth (m)

The two-dimensional Vs section along Line A (Fig. 13) reveals pronounced lateral heterogeneity in subsurface structure. Low-velocity layers dominate the shallow subsurface and exhibit considerable thickness variations along the profile. A notable thickening of low- to intermediate-velocity sediments is observed between stations SP_A11 and SP_A15, indicating the presence of a relatively deeper sedimentary accumulation compared to adjacent areas. This zone corresponds to a significant change in subsurface geometry and is marked by a sharp transition between low- and high-velocity units. In contrast, the southern segment of Line A, particularly near

SP_A01 to SP_A04, shows a shallower transition to high-Vs layers, suggesting that bedrock or compact material occurs at relatively shallow depths. The abrupt changes in layer geometry along Line A indicate significant lateral variations in subsurface mechanical properties.

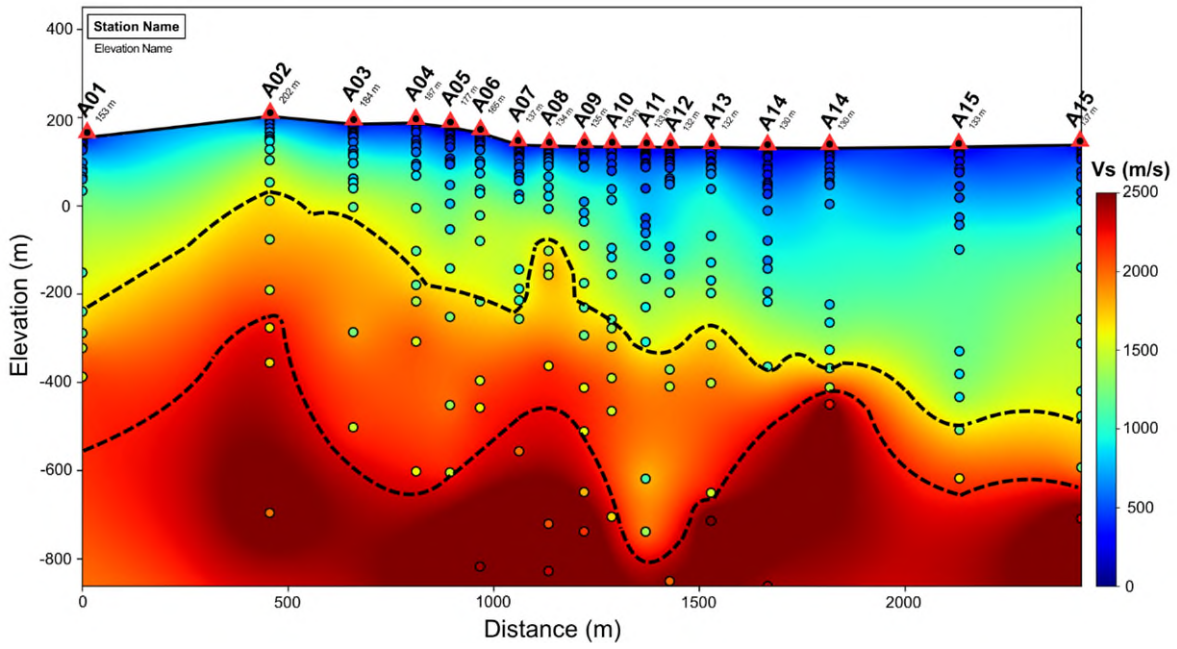


Fig. 13 Two-dimensional shear-wave velocity (Vs) section derived from HVSR inversion along Line A. Colors represent the spatial distribution of Vs values, ranging from low velocities (soft sediments) to high velocities (stiff materials or bedrock). Red triangles indicate microtremor measurement stations used for model construction. Colored circular nodes represent inversion control points at each station. Dashed black lines indicate interpreted boundaries between major subsurface units based on significant changes in velocity gradients

Compared to Line A, the two-dimensional Vs section along Line B (Fig. 14) exhibits a relatively more uniform velocity structure, although lateral variations remain evident. Shallow low-Vs layers are still present throughout the profile, but their thickness is generally thinner than those observed along Line A. A localized thickening of low-velocity material occurs near the central part of the line, particularly around SP_B04 to SP_B06, whereas both western and eastern sections show shallower high-Vs layers. Overall, the inversion-derived Vs models reveal substantial variations in sediment thickness, bedrock depth, and subsurface stiffness across the study area. These results document lateral variations in sediment thickness, velocity, and inferred subsurface boundaries that are evaluated further in the structural interpretation. Similar studies by Stephenson et al. (2022) demonstrated that integrating HVSR analysis with Vs inversion can improve the characterization of sedimentary structure and bedrock geometry.

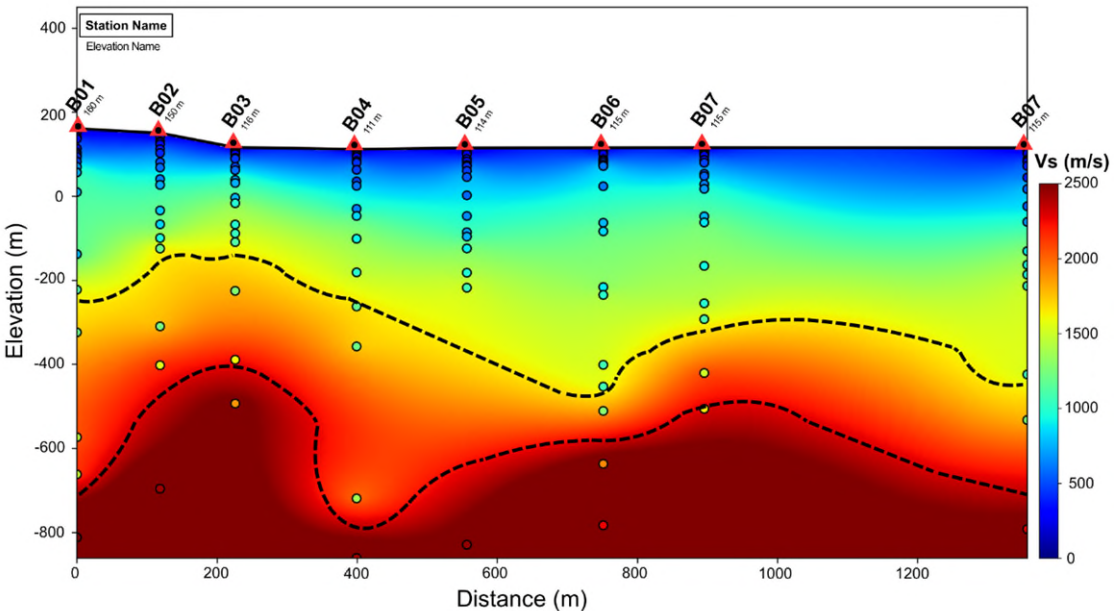


Fig. 14 Two-dimensional shear-wave velocity (Vs) section derived from HVSR inversion along Line B. Colors represent the spatial distribution of Vs values, ranging from low velocities to high velocities. Red triangles indicate microtremor measurement stations. Colored circular nodes represent inversion control points. Dashed black lines indicate interpreted boundaries between major subsurface units based on significant changes in velocity gradients. The section illustrates lateral variations in sediment thickness and bedrock geometry along Line B

5 Discussion

5.1 Spatial Variability of HVSR Parameters and Fault-Controlled Elastic Heterogeneity

The spatial variability in HVSR parameters may reflect differences in sediment thickness, lithology, and possible deformation-related heterogeneity. Although dominant frequency (f_0) and peak amplification (A_0) are commonly associated with resonance characteristics and impedance contrasts, their localized distribution suggests that tectonic deformation has progressively modified the elastic properties of the near-surface materials. Fault-related fracturing, weathering, and fluid circulation are known to reduce rock stiffness and increase impedance contrasts, producing measurable variations in ambient vibration responses (Nakamura, 2000; Stephenson et al., 2022; Vijayan et al., 2022). Consequently, the heterogeneous velocity structure identified beneath the study area may reflect the combined influence of geological variations and fault-related deformation processes associated with the Palolo Fault.

The concentration of low-frequency responses accompanied by relatively elevated seismic vulnerability indices further implies the presence of mechanically weakened zones within the investigated fault corridor. Similar patterns have been reported in active fault environments where cumulative brittle deformation generates fractured rocks with reduced shear modulus, leading to lower resonance frequencies and stronger site amplification compared with adjacent intact blocks (Tal and Faulkner, 2022). Rather than representing isolated

anomalies, these variations collectively suggest that the Palolo Fault is characterized by spatially variable deformation intensity, reflecting differences in strain localization and fault damage development along the investigated segment.

These observations demonstrate that HVSR-derived parameters can provide geological information extending beyond conventional site-response assessment. When interpreted together with subsurface velocity models, the spatial organization of resonance characteristics offers valuable constraints on the distribution of mechanically weakened domains and provides an initial framework for identifying fault-controlled heterogeneity within active tectonic environments. Such an interpretation is particularly advantageous in regions where dense vegetation, weathering, or limited outcrop exposure restrict direct geological observations.

5.2 Geological Significance of Shear-Wave Velocity Variations

Shear-wave velocity variations provide important constraints on the mechanical evolution of the Palolo Fault because Vs is directly related to the stiffness and degree of consolidation of subsurface materials. In tectonically active settings, spatial heterogeneity in Vs commonly reflects the cumulative effects of brittle deformation, weathering, and fluid-rock interactions rather than lithological variability alone. Repeated fault activity progressively increases fracture density and rock permeability, promoting mechanical weakening that is expressed as localized low-velocity domains within the fault zone (Delorey et al., 2021; Tal and Faulkner, 2022). Consequently, the heterogeneous velocity structure identified beneath the study area likely records the long-term evolution of deformation associated with the Palolo Fault.

The observed lateral variability in shear-wave velocity also suggests that tectonic strain has not been accommodated uniformly throughout the investigated fault segment. Instead, deformation appears to have been preferentially localized within discrete structural domains, producing zones with contrasting mechanical properties over relatively short distances. Such mechanical segmentation is widely recognized in mature fault systems, where fault activity is distributed between principal fault cores and surrounding damage zones rather than occurring along a single continuous fault plane. This interpretation implies that the present-day subsurface architecture of the Palolo Fault reflects spatially variable deformation intensity, with mechanically weakened zones representing locations where cumulative strain has been concentrated during fault evolution.

From a geological perspective, the distribution of shear-wave velocity provides more than a description of subsurface layering. Variations in Vs offer insight into the mechanical behavior of the fault zone by delineating transitions between relatively competent rocks and deformation-weakened materials. Integrating these velocity variations with HVSR-derived resonance characteristics therefore provides a more comprehensive framework for

evaluating fault-controlled elastic heterogeneity and improves the interpretation of subsurface structures in tectonically active regions.

5.3 Implications of Two-Dimensional Vs Models for Fault Architecture

The two-dimensional shear-wave velocity models provide additional constraints by highlighting subsurface velocity discontinuities that are not directly visible in the available surface observations. As illustrated in Fig. 15, several velocity boundaries are abruptly displaced and interrupted over relatively short lateral distances, producing discontinuous subsurface geometries that are inconsistent with laterally continuous sedimentary deposition Such abrupt changes may indicate tectonic discontinuities, although variations in lithology, sediment thickness, or weathering conditions may also contribute to these velocity contrasts and modifies the continuity of subsurface mechanical properties.

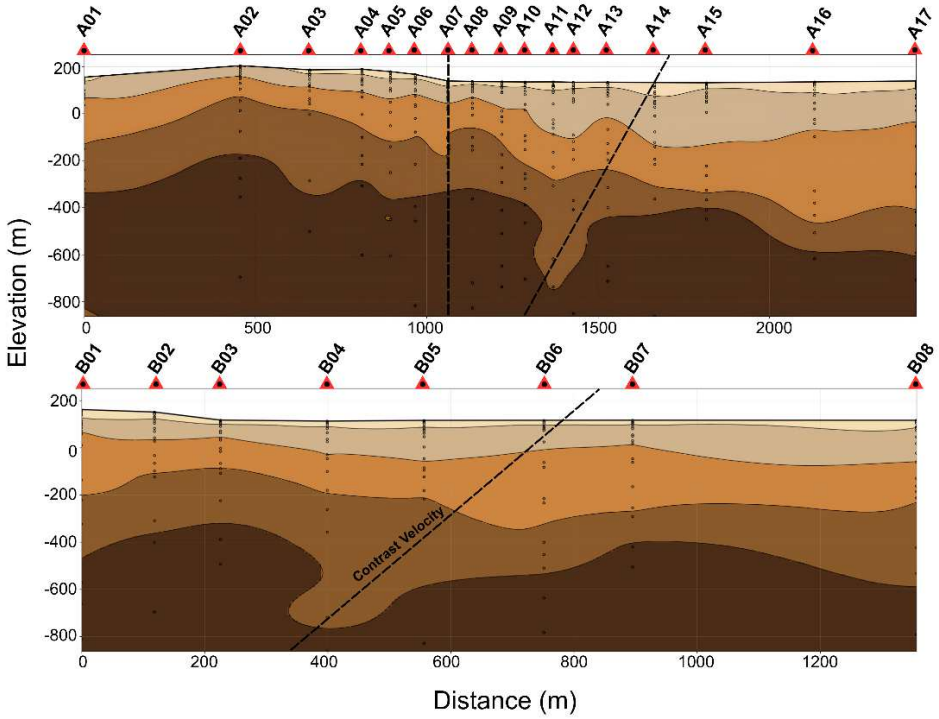


Fig. 15 Classification of subsurface velocity units derived from two-dimensional shear-wave velocity (Vs) models along (a) Line A and (b) Line B. The subsurface structure is classified into five velocity units based on Vs values. Unit 1 represents unconsolidated to soft sediments near the surface, whereas Units 4–5 correspond to compact materials and engineering bedrock. Red triangles indicate microtremor measurement stations used for model construction. Black dashed lines mark zones of significant lateral velocity discontinuity interpreted as potential structural boundaries or fault-related deformation zones. The classification highlights the spatial variation of sediment thickness, subsurface stiffness, and bedrock geometry across the study area

The interpreted discontinuities are accompanied by localized low-velocity corridors that persist across several interpolated depth levels (Fig. 16). This configuration is compatible with a deformation-related low-velocity zone, although lithological changes, weathering, and interpolation effects may produce similar patterns, where repeated brittle deformation increases fracture density and weathering intensity, resulting in reduced elastic stiffness relative to the surrounding rocks. Rather than representing isolated lithological variations, these vertically persistent anomalies indicate that deformation has remained localized within narrow structural corridors over multiple stages of fault evolution. Similar low-velocity features have been reported in active fault systems where shear-wave velocity models successfully delineate concealed fault traces and subsidiary deformation zones beneath areas with limited surface expression (Liu et al., 2022).

An additional implication of the velocity models is that deformation within the investigated segment of the Palolo Fault appears to be distributed across multiple structural discontinuities rather than accommodated by a single fault plane. The occurrence of several offsets in Fig. 16 suggest possible structural discontinuities that may warrant further investigation as subsidiary fault-related features which collectively form a broader deformation zone. Such structural complexity is consistent with conceptual models of mature fault evolution, in which cumulative displacement is partitioned into fault cores, splays, relay structures, and surrounding damage zones instead of remaining confined to one principal fault surface. Accordingly, the interpreted velocity architecture supports the view that the Palolo Fault comprises multiple mechanically distinct domains that have evolved through progressive tectonic deformation.

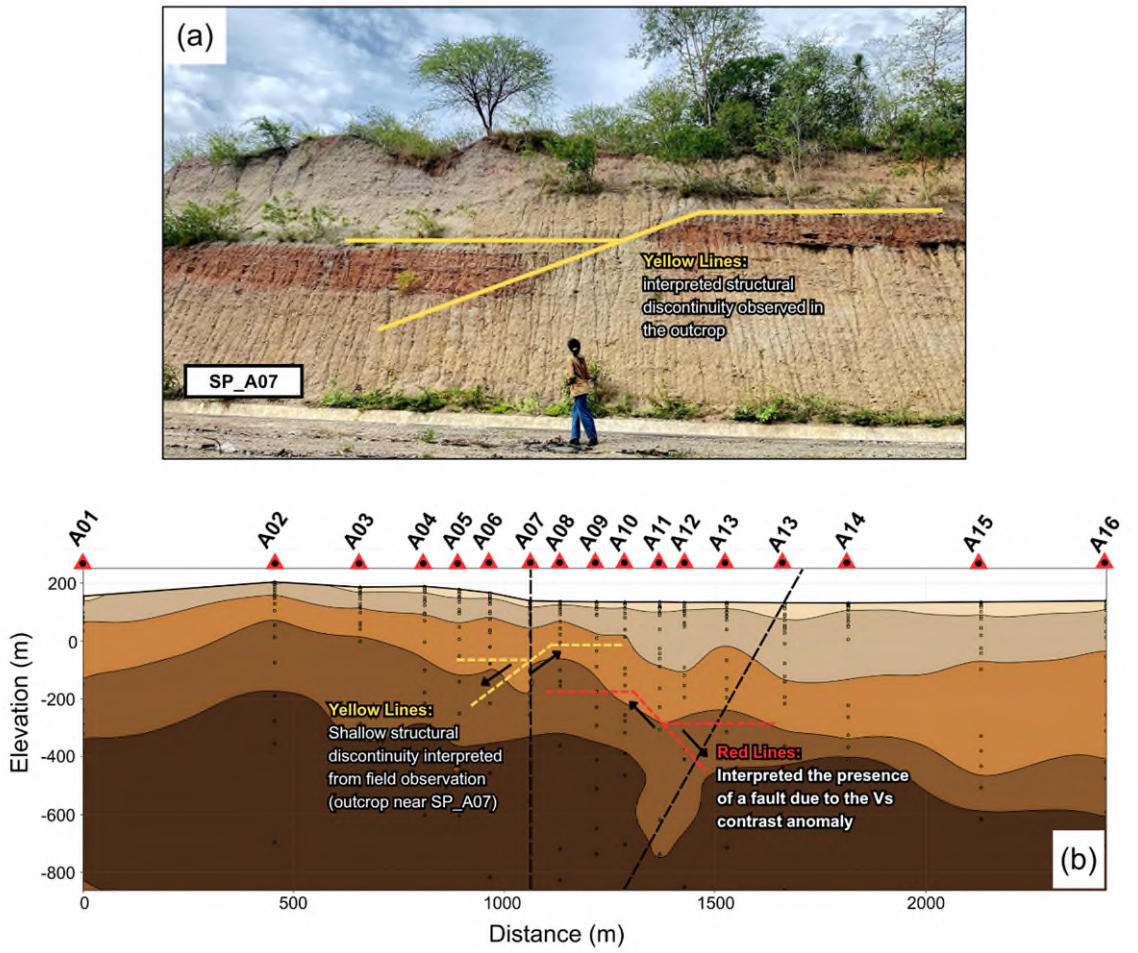


Fig. 16 Integrated geological and geophysical evidence may indicate the presence of a fault due to the Vs contrast anomaly interpretation along Line A. (a) Interpreted outcrop highlighting a structural discontinuity (yellow lines), indicating deformation within near-surface sedimentary deposits, (b) Correlation between field observation and the two-dimensional Vs model along Line A, showing interpreted Correlation between field observation and the two-dimensional Vs model along Line A, showing interpreted may indicate the presence of a fault due to the Vs contrast anomaly. Yellow dashed lines represent shallow structural discontinuities observed in the outcrop, while red dashed lines indicate inferred deeper fault-related deformation zones based on abrupt lateral velocity contrasts and offsets in subsurface velocity units. Black dashed vertical lines mark interpreted fault positions associated with significant changes in subsurface geometry. The combined geological and geophysical may indicate the presence of a fault due to the Vs contrast anomaly that likely developed as secondary deformation structures associated with the regional Palolo Fault system.

Conclusion

The integration of ambient vibration measurements with HVSR inversion provides a practical framework for characterizing near-surface elastic heterogeneity across the investigated Palolo Fault segment. Rather than serving solely as a site-response assessment technique, HVSR-derived shear-wave velocity models effectively resolve variations in subsurface mechanical properties, allowing fault-controlled heterogeneity to be distinguished from regional lithological variability. The identified structural discontinuities may indicate that deformation within the

investigated area is accommodated through a structurally complex fault zone composed of multiple mechanically distinct domains rather than a single continuous fault plane.

Some velocity anomalies occur outside the mapped surface trace of the Palolo Fault, but their structural significance remains uncertain, with localized velocity anomalies that may be related to structural deformation modifying the shallow subsurface geometry and mechanical properties. These findings highlight the value of integrating HVSR analysis with two-dimensional velocity modelling for improving the characterization of concealed fault architecture and provide additional geophysical information that may be useful for subsequent geological and site-response investigations in tectonically active regions.

This interpretation remains subject to several limitations. The subsurface architecture presented here is derived from two-dimensional HVSR inversion and therefore represents a simplified approximation of a potentially three-dimensional fault system. In addition, the inferred structural discontinuities are based primarily on geophysical evidence and have not yet been independently validated using borehole data, active seismic surveys, or trench investigations.

Future studies should integrate HVSR-derived velocity models with complementary geophysical, geological, and geotechnical datasets to improve the resolution of fault geometry and deformation patterns. Three-dimensional velocity modelling, denser measurement networks, and direct structural validation are expected to provide a more comprehensive understanding of the internal architecture and evolutionary history of the Palolo Fault.

Acknowledgement

The authors would like to express their sincere gratitude to the Meteorological, Climatological, and Geophysical Agency (BMKG) for its support and for providing access to the data and facilities that contributed to this study. The authors also sincerely thank the Department of Geophysics, Faculty of Mathematics and Natural Sciences, Hasanuddin University, for its academic support and research facilities throughout this work. Special appreciation is extended to the Palu Internship Team for their invaluable assistance during the field survey and data acquisition. The authors are particularly grateful to Sthevy Firstien Atabui and Fahreezy Arthur Ridho for their support during field activities and technical assistance. The authors also acknowledge the members of Ankes Andri Geophysics Laboratory Team for their continuous support, constructive discussions, and assistance throughout the research process.

CrediT authorship contribution statement

All authors contributed to the conception and design of the study. Zalsa Nabila HR led the research, conducted fieldwork, performed data processing and analysis, interpreted the results, and prepared the initial manuscript. Valensya Arruan Silomba contributed to data processing, visualization, figure preparation, and manuscript drafting. Nurul Maghfirah and Samida Danda contributed to data interpretation, manuscript drafting, and validation of the research findings. Andri Moh. Wahyu Laode supervised the research, validated the methodology and interpretation, and critically revised the manuscript. Muhammad Altin Massinai provided scientific supervision and contributed to the conceptual development of the study. Muh. Farid Wajedy and Sofian provided scientific supervision and critically reviewed the manuscript. All authors read and approved the final version of the manuscript.

Funding

The study was conducted independently and received no financial support from public, commercial, or charitable organizations.

Data availability

The data that support the findings of this study are available from the corresponding author upon reasonable request.

Conflict of interest

The authors declare that they have no known competing financial interests or personal relationships that could have appeared to influence the work reported in this study.

References

Abdelrahman, K., 2025. Shear wave velocity structure at King Saud University, Saudi Arabia, derived from MASW and microtremor arrays. Sci. Rep. 15, 1–22. https://doi.org/10.1038/s41598-025-90894-4

Abdelrahman, K., Alarifi, S.S., 2026. Scientific Reports Article in Press Dense MASW shear-wave imaging of weak-zone networks and preferential leachate pathways beneath rumah landfill site , central saudi arabia IN IN. Sci. Rep. https://doi.org/https://doi.org/10.1038/s41598-026-54326-1

Abdelrahman, K., Saadon, A.B., Qaysi, S., 2024. Estimating shear wave velocity and site characterization of western Riyadh City , Saudi Arabia based on multichannel analysis of surface waves 1–23. https://doi.org/10.3389/feart.2024.1395431

Aditama, M.R., Laksono, F.A.T., Fadlin, Purwasatriya, E.B., Kovács, J., Mishra, M., 2025. Structural framework and fault seal prediction of the central slyne basin prospect, Irish Atlantic margin. Geo-Marine Lett. 45, 1–14. https://doi.org/10.1007/s00367-025-00804-w

Ai, H., Abdelrahman, K., Eldosouky, A.M., 2026. and joint inversion of surface wave dispersion and earthquake-based HVSR by MBMO for obtaining reliable subsurface structures.

Akin, O., Hakan, K., Muhammet, C., Sunnetci, O., Senkaya, M., Sayil, N., 2026. Assesment of landslide susceptibility through analytical hierarchy process including surface wave data for Trabzon Degirmendere Valley (NE Türkiye).

Avila, V, R., Perton, M., Aguirre, J., 2025. ground motion amplification r e vealed by the Xochimilco ambient. Geophys. J. Int. 241, 1988–2002. https://doi.org/10.1093/gji/ggaf139

Barone, I., Boaga, J., Carrera, A., Flores-Orozco, A., Cassiani, G., 2021. Tackling Lateral Variability Using Surface Waves: A Tomography-Like Approach. Surv. Geophys. 42, 317–338. https://doi.org/10.1007/s10712-021-09631-x

Bedford, J.D., Faulkner, D.R., Lapusta, N., 2022. Fault rock heterogeneity can produce fault weakness and reduce fault stability. Nat. Commun. 13, 1–7. https://doi.org/10.1038/s41467-022-27998-2

Boumpoulis, V., Michalopoulou, M., Depountis, N., 2023. Comparison between different spatial interpolation methods for the development of sediment distribution maps in coastal areas. Earth Sci. Informatics 2069–2087. https://doi.org/10.1007/s12145-023-01017-4

Bruno, P.P.G., Ferrara, G., Improta, L., 2025. 3D High-Resolution Seismic Imaging of Elusive Seismogenic Faults : The Pantano-Ripa Rossa Fault , Southern Italy 1–28.

Caputo, R., Improta, L., Maraio, S., Giulio, G. Di, Vassallo, M., Massa, M., Lovati, S., Lupi, M., Villani, F., Hailemikael, S., Famiani, D., Mercuri, A., Martini, P.M. De, Sapia, V., Alessandro, A.D., Paolo, P., Bruno, G., Brunori, C.A., Civico, R., Sciarra, A., Roselli, P., Figlioli, A., Bongiovanni, S., Pucillo, S., Riccio, G., Cogliano, R., Brunelli, G., Scudero, S., Speciale, S., Ruggiero, L., Baccheschi, P., Cultrera, G., Pucci, S., Valoroso, L., Gori, P. De, 2026. Characterizing the subsurface structure and active faults of the Fucino Basin (Central Apennines) through integrated high-resolution seismic reflection and nodal ambient noise surveys 1–25. https://doi.org/10.3389/feart.2026.1778360

Chen, S., Gao, R., Lu, Z., Liang, Y., Cai, W., Cao, L., Chen, Z., 2023. Shear wave velocity structure of the upper crust in north Xiaojiang fault zone in SE Tibet via short-period ambient noise dense seismic array. Phys. Earth Planet. Inter. 344, 107110. https://doi.org/10.1016/j.pepi.2023.107110

Cherki, F., Raki, A., Tadili, M., Tadili, B., Mhammdi, N., 2026. Horizontal-to-vertical spectral ratio-based seismic site characterization of the Agadir Oufella area , southwestern Morocco 27, 415–425.

Dabhi, D., Pandya, K., 2020. Uncertain Scenario Based MicroGrid Optimization via Hybrid Levy Particle Swarm Variable Neighborhood Search Optimization (HL _ PS _ VNSO) 8. https://doi.org/10.1109/ACCESS.2020.2999935

de la Torre, C.A., Bradley, B.A., Megann, C.R., 2022. 2D Geotechnical Site-Response Analysis including Soil Heterogeneity and Wave Scattering. Earthq. Spectra 38. https://doi.org/https://doi.org/10.1177/87552930211056667

Delorey, A.A., Guyer, R.A., Bokelmann, G.H.R., Johnson, P.A., 2021. Probing the Damage Zone at Parkfield. Geophys. Res. Lett. 48, 1–9. https://doi.org/10.1029/2021GL093518

Duwiquet, H., Guillou-frottier, L., Arbaret, L., Bellanger, M., Guillon, T., Heap, M.J., 2021. Crustal Fault Zones (CFZ) as Geothermal Power Systems : A Preliminary 3D THM Model Constrained by a Multidisciplinary Approach 2021. https://doi.org/10.1155/2021/8855632

Elfadly, M.A., Abdelrady, M., Decarlis, A., Ibraheem, I.M., Shebl, A., 2026. Multidisciplinary approaches to lithological discrimination and structural mapping for mineral resource assessment 1–32.

Feng, S., Yang, D., Jiang, F., Yu, C., Liu, X., Liu, M., 2026. Jo ur na l P re. Earthq. Res. Adv. 100456. https://doi.org/10.1016/j.eqrea.2026.100456

Fichtner, A., Zunino, A., Gebraad, L., Boehm, C., 2021. Autotuning Hamiltonian Monte Carlo for efficient generalized nullspace exploration 941–968.

Frando, M., Ariyanto, P., Purba, J., Apriliaji, T.M., 2025. Gravity-anomaly-based analysis of surface ruptures along the Palu-Koro Fault (Indonesia) for long-term seismic hazard mitigation. Bull. Geogr. Phys. Geogr. Ser. 28, 81–101. https://doi.org/10.12775/bgeo-2025-0006

Galone, L., Amico, S.D., Fucks, E., Colica, E., Carol, E., Rivero, L., Panzera, F., Laura, M., 2026. Ambient-Noise HVSR signatures of deep and shallow impedance structure in a quaternary Plain (Pampean Region , Argentina). J. Appl. Geophys. 250, 106225. https://doi.org/10.1016/j.jappgeo.2026.106225

Gosselin, J.M., Dosso, S.E., Askan, A., Wathelet, M., Savvaidis, A., Cassidy, J.F., 2022. A review of inverse methods in seismic site characterization. Journal of Seismology.

Gupta, R.K., Agrawal, M., Pal, S.K., Das, M.K., 2021. Seismic site characterization and site response study of Nirsa (India). Nat. Hazards 108, 2033–2057. https://doi.org/10.1007/s11069-021-04767-w

Huang, D., Wang, G., Du, C., Jin, F., 2019. Seismic Amplification of Soil Ground with Spatially Varying Shear

626 Wave Velocity Using 2D Spectral Element Method Seismic Ampli fi cation of Soil Ground with Spatially
627 Varying Shear Wave Velocity Using 2D Spectral Element Method. J. Earthq. Eng. 0, 1–16.
628 https://doi.org/10.1080/13632469.2019.1654946
629 Janssens, U., 2024. Functional hemodynamic monitoring. Medizinische Klin. - Intensivmed. und Notfallmedizin.
630 https://doi.org/10.1007/s00063-024-01190-4
631 Juan, A.A., Keenan, P., Martí, R., Mcgarraghy, S., Panadero, J., Carroll, P., Oliva, D., 2021. A review of the role
632 of heuristics in stochastic optimisation : from metaheuristics to learnheuristics. Ann. Oper. Res.
633 https://doi.org/10.1007/s10479-021-04142-9
634 Kang, S.Y., Kim, K.H., Chiu, J.M., Liu, L., 2020. MicrotremorHVSR analysis of heterogeneous shallow
635 sedimentary structures at Pohang, South Korea. J. Geophys. Eng. 17, 861–869.
636 https://doi.org/10.1093/jge/gxaa035
637 Keil, S., Wassermann, J., 2023. Surface w av e dispersion curv e inv ersion using mixture density networks 401–
638 415.
639 Kim, G., Lee, J., Hwang, S., Stokoe, K.H., 2026. Jo ur l P re r f. J. Rock Mech. Geotech. Eng.
640 https://doi.org/10.1016/j.jrmge.2026.03.023
641 Kong, W., Tan, H., Lin, C., Unsworth, M., 2021. Three-Dimensional Inversion of Magnetotelluric Data for a
642 Resistivity Model With Arbitrary Anisotropy Journal of Geophysical Research : Solid Earth 1–22.
643 https://doi.org/10.1029/2020JB020562
644 Krylov, A.A., Kulikov, M.E., Kovachev, S.A., Medvedev, I.P., Lobkovsky, L.I., Semiletov, I.P., 2022.
645 Peculiarities of the HVSR Method Application to Seismic Records Obtained by Ocean-Bottom
646 Seismographs in the Arctic. Appl. Sci. 12, 1–22.
647 Laby, D.A., Sungkono, S., Biswas, A., 2025. Regularized ensemble Kalman inversion for robust and efficient
648 gravity data modeling to identify mineral and ore deposits 1–31.
649 Lacombe, O., Tavani, S., Lamarche, J., Balsamo, F., Agosta, F., 2023. Introduction : Faults and fractures in rocks :
650 mechanics , occurrence , dating , stress history and fluid flow.
651 Li, M., Yao, H., Feng, J., Zeng, X., Luo, G., Wang, C., 2025. Crustal deformation characteristics and tectonic
652 implications on the northeastern margin of the Tibetan Plateau. Phys. Earth Planet. Inter. 366, 107420.
653 https://doi.org/10.1016/j.pepi.2025.107420
654 Liu, X., Beroza, G.C., Ben-Zion, Y., 2022. Ambient Noise Attenuation Tomography Reveals an Asymmetric
655 Damage Zone Across San Jacinto Fault Near Anza, California. Geophys. Res. Lett. 49, 1–9.

https://doi.org/10.1029/2022GL099562

Medwedeff, W.G., Clark, M.K., Zekkos, D., West, A.J., Chamlagain, D., 2021. Near-Surface Geomechanical Properties and Weathering Characteristics Across a Tectonic and Climatic Gradient in the Central Nepal Himalaya Journal of Geophysical Research : Earth Surface. J. Geophys. Res. Earth Surf. 127, 1–23. https://doi.org/10.1029/2021JF006240

Meng, Q., Li, Y., Wang, W., Chen, Y., Wang, S., 2023. A Case Study Assessing the Liquefaction Hazards of Silt Sediments Based on the Horizontal-to-Vertical Spectral Ratio Method. J. Mar. Sci. Eng. 11. https://doi.org/10.3390/jmse11010104

Mi, B., Xia, J., Bradford, J.H., Shen, C., 2020. Estimating Near - Surface Shear - Wave - Velocity Structures Via Multichannel Analysis of Rayleigh and Love Waves : An Experiment at the Boise Hydrogeophysical Research Site. Surv. Geophys. https://doi.org/10.1007/s10712-019-09582-4

Mianshui, R., Li-yun, F., Weijia, S., 2022. Joint inversion of horizontal-to-vertical spectral ratio and phase velocity dispersion : Applications to Garner Valley 1–18. https://doi.org/10.3389/feart.2022.948697

Molnar, S., Sirohey, A., Assaf, J., Bard, P.-Y., Castellaro, S., Cornou, C., Cox, B., Guillier, B., Hassani, B., Kawase, H., Matsushima, S., Sanchez-Sesma, F.J., Yong, A., 2022. A review of the microtremor horizontal - to - vertical spectral ratio (MHVSR) method. J. Seismol. 26, 653–685. https://doi.org/10.1007/s10950-021-10062-9

Nagamani, D., Sivaram, K., Rao, N.P., Satyanarayana, H.V.S.S., 2020. Ambient noise and earthquake HVSR modelling for site characterization in southern mainland, Gujarat. J. Earth Syst. Sci. 129. https://doi.org/10.1007/s12040-020-01443-8

Nakamura, Y., 2000. Clear Identification of Fundamental Idea of Nakamura ' S. Spectrum 2656.

Nardone, L., Esposito, R., Galluzzo, D., Petrosino, S., Cusano, P., Rocca, M. La, 2020. Array and spectral ratio techniques applied to seismic noise to investigate the Campi Flegrei (Italy) subsoil structure at different scales 75–85.

Nuarta, I.K., Janat, N.R., Abdullah, A.I., Asrafil, Mukaddas, A., 2024. Penentuan Kestabilan Lereng Batuan Menggunakan Limit Equilibrium Method (LEM) Di Ruas Jalan Trans Palu-Kulawi Desa Salua Kabupaten Sigi. Media Konstr. 9, 417–432. https://doi.org/10.33772/jmk.v9i4.147

Olafsdottir, E.A., Erlingsson, S., 2020. Open-Source MASW Inversion Tool Aimed at Shear Wave Velocity Profiling for Soil Site Explorations 22–25.

Olivares-palomares, Á.B., Aguirre, J., Ramirez-guzman, L., 2025. Southern Mexico City Shear-Wave Velocity

686 Estimation Using Ambient Seismic Noise. https://doi.org/10.1785/0220240488.Supplemental
687 Panadero, J., Doering, J., Kizys, R., Juan, A.A., Fito, A., 2018. A variable neighborhood search simheuristic for
688 project portfolio selection under uncertainty. J. Heuristics. https://doi.org/10.1007/s10732-018-9367-z
689 Patria, A., Putra, P.S., 2020. Development of the Palu – Koro Fault in NW Palu Valley , Indonesia. Geosci. Lett.
690 1–11. https://doi.org/10.1186/s40562-020-0150-2
691 Patria, A., Titu-eki, A., Daryono, M.R., 2026a. New Insights into Active Faulting in Sulawesi , Indonesia Research
692 Paper Journal of Engineering and Technological Sciences 58, 121–138.
693 https://doi.org/10.5614/j.eng.technol.sci.2025.58.1.9
694 Patria, A., Titu-Eki, A., Daryono, M.R., 2026b. New Insights into Active Faulting in Sulawesi, Indonesia. J. Eng.
695 Technol. Sci. 58, 121–138. https://doi.org/10.5614/j.eng.technol.sci.2026.58.1.9
696 Pereira, M.L., Fernandes, I., Costa, M., Pappalardo, L., Zanon, V., Amaral, P., 2026. Engineering Properties of
697 Lava Rocks from S . Miguel Island : Insights from Laboratory Testing and New Empirical Correlations.
698 Rock Mech. Rock Eng. https://doi.org/10.1007/s00603-026-05348-8
699 Perez, C.J.A., 2024. Reevaluating soil amplification using multi - spectral HVSR technique in La Chana
700 Neighborhood , Granada , Spain. J. Seismol. 28, 921–949. https://doi.org/10.1007/s10950-024-10227-2
701 Pischiutta, M., Salvini, F., Fletcher, J., Rovelli, A., 2012. at Fremont , California : dominant fault-high-angle
702 polarization and 1255–1272. https://doi.org/10.1111/j.1365-246X.2011.05319.x
703 Project, S.E., 2004. Guidelines for The Implementation Of The H / V Spectral Ratio Technique on Ambient
704 Vibrations Measurements , Processing and Interpretation. European Commission – Research General
705 Directorate.
706 Provenzano, G., Ludovic, M., 2025. Geophysical Journal International 1–19. https://doi.org/10.1093/gji/ggaf354
707 Purba, J., Priadi, R., Wulur, K.H.C., Pertiwi, I.I., 2026. Investigating Stress Transfer and Fault Interaction in the
708 July-August 2025 Poso and Tokararu Earthquakes, Central Sulawesi, Indonesia. Ann. Geophys. 69, 1–18.
709 https://doi.org/10.4401/ag-9425
710 PuSGeN, 2025. PETA SUMBER DAN BAHAYA GEMPA INDONESIA TAHUN 2024, Edisi 1. ed. Kementrian
711 Pekerjaan Umum, Jakarta.
712 Rahayu, T., Nasution, Z., Roesyanto, Karnawati, D., 2022. Regional zonation based on seismic vulnerability using
713 local site effect analysis and potential damage to the city of Medan (North Sumatra, Indonesia) due to
714 earthquake. Geoenvironmental Disasters 9. https://doi.org/https://doi.org/10.1186/s40677-022-00227-0
715 Rahimi, S., Wood, C.M., Bernhardt-barry, M., 2021. The MHVSR technique as a rapid , cost-effective , and

716 noninvasive method for landslide investigation : case studies of Sand Gap and Ozark , AR , USA.
717 https://doi.org/10.1007/s10346-021-01677-7
718 Rigo, A., Sokos, E., Lefils, V., Briole, P., 2021. Seasonal variations in amplitudes and resonance frequencies of
719 the HVSR amplification peaks linked to groundwater. Geophys. J. Int. 226, 1–13.
720 https://doi.org/10.1093/gji/ggab086
721 Rohit, D., Hazarika, H., Maeda, T., Sumartini, W.O., Kokusho, T., Manafi Khajeh Pasha, S., Nurdin, S., 2021.
722 Forensic investigation of flowslides triggered by the 2018 Sulawesi earthquake. Prog. Earth Planet. Sci. 8.
723 https://doi.org/10.1186/s40645-021-00452-5
724 Rong, M., Li, X., Fu, L., 2021. Improvement of the objective function in the velocity structure inversion based on
725 horizontal-to-vertical spectral ratio of earthquake ground motions. Geophys. J. Int. 224, 1–16.
726 https://doi.org/10.1093/gji/ggaa347
727 Rosalia, S., Widiyantoro, S., Cummins, P.R., Yudistira, T., Nugraha, A.D., Zulfakriza, Z., Setiawan, A., 2022.
728 Upper crustal shear-wave velocity structure Beneath Western Java, Indonesia from seismic ambient noise
729 tomography. Geosci. Lett. 9, 1–14. https://doi.org/10.1186/s40562-021-00208-5
730 Rosid, M.S., Nursarifa, S., Riyanto, A., 2023. Identification of Geological Structures in Sigi Regency, Central
731 Sulawesi Based on Derivative Analysis of Gravity Data. Int. J. GEOMATE 24, 26–33.
732 https://doi.org/10.21660/2023.103.3426
733 Scarponi, M., Kvapil, J., Plomerov, J., Solarino, S., 2024. New constraints on the shear w av e v elocity structur
734 e of the Ivr ea geoph ysical bod y fr om seismic ambient noise tomograph y (Ivrea-Verbano Zone , Alps)
735 1089–1105.
736 Seivane, H., Garc, A., Navarro, M., Molina, L., Navarro-mart, F., 2022. On the use of the microtremor HVSR for
737 tracking velocity changes : a case study in Campo de Dal ´ ıas basin (SE Spain) 542–564.
738 Serhalawan, Y., Chen, P., 2024. Tectonophysics Seismotectonics of Sulawesi , Indonesia. Tectonophysics 883.
739 https://doi.org/https://doi.org/10.1016/j.tecto.2024.230366
740 Shu, J., Li, Y., 2026. Research progress and current status of dynamic wave propagation characteristics in rock
741 mass : A review 1–33. https://doi.org/10.1002/dug2.70080
742 Sibson, R.H., 2020. Preparation zones for large crustal earthquakes consequent on fault - valve action. Earth,
743 Planets Sp. https://doi.org/10.1186/s40623-020-01153-x
744 Silahtar, A., Budakoğlu, E., Kafadar, Ö., Şenkaya, M., 2026. Characterizing soil dynamic parameters through
745 ambient seismic noise in the Sakarya region of the north anatolian fault system.

Silahtar, A., Karaaslan, H., Kocaman, K., Senkaya, M., Albayrak, F., 2025. Multi-criteria microzonation Hazard assessment based on the analytic hierarchy process framework. Geomatics, Nat. Hazards Risk 16. https://doi.org/10.1080/19475705.2025.2584701

Song, Y., Gong, F., Zeng, L., Zhang, Z., Mao, Z., Huang, C., Yao, Y., Tan, X., Lin, B., 2024. modelling perspective 1165–1180.

Stanko, D., Markušić, S., 2020. An empirical relationship between resonance frequency, bedrock depth and VS30 for Croatia based on HVSR forward modelling. Nat. Hazards 103, 3715–3743. https://doi.org/10.1007/s11069-020-04152-z

Stephenson, W.J., Yong, A., Martin, A., 2022. Flexible multimethod approach for seismic site characterization. J. Seismol. 26, 687–711. https://doi.org/10.1007/s10950-022-10102-y

Syamsuddin, E., Moh, A., Laode, W., Muhamad, A., Sutadi, H., 2026. Temporal evolution of site response in Petobo ' s post-liquefaction zone , Palu , Indonesia : A comparative HVSR curve analysis. Soil Dyn. Earthq. Eng. 203, 110117. https://doi.org/10.1016/j.soildyn.2026.110117

Tal, Y., Faulkner, D., 2022. The Effect of Fault Roughness and Earthquake Ruptures on the Evolution and Scaling of Fault Damage Zones. J. Geophys. Res. Solid Earth 127, 1–19. https://doi.org/10.1029/2021JB023352

Tan, L., He, R., Tang, H., Li, Y., Li, Z., 2026. Intra-crustal shear wave structures and metallogenic features in the Gerze Area , Tibet : constrained by Rayleigh wave tomography. Ore Geol. Rev. 193, 107320. https://doi.org/10.1016/j.oregeorev.2026.107320

Tang, Z., Julià, J., Mai, P.M., Mooney, W.D., Wu, Y., 2022. Shear-Wave Velocity Structure Beneath Northeast China From Joint Inversion of Receiver Functions and Rayleigh Wave Phase Velocities : Implications for Intraplate Volcanism Journal of Geophysical Research : Solid Earth 1–26. https://doi.org/10.1029/2022JB023956

Tarabusi, G., Sgattoni, G., Caputo, R., 2024. Imaging buried anticlines in the Po Plain , northern Italy , based on HVSR frequency and amplitude analyses. Int. J. Earth Sci. 113, 1457–1473. https://doi.org/10.1007/s00531-024-02448-0

Tawil, S., 2024. Morphotectonic Analysis in the Sombe Lewara Sub-Watershed in the Region of Palu City and Sigi Regency, Central Sulawesi Province. Int. J. Curr. Sci. Res. Rev. 07, 2485–2495. https://doi.org/10.47191/ijcsrr/v7-i5-08

Vantassel, J.P., Cox, B.R., 2021. SWinvert : a workflow for performing rigorous 1-D surface wave inversions 1141–1156. https://doi.org/10.1093/gji/ggaa426

Vergara-huerta, F., Aguirre, J., 2020. One-dimensional seismic velocity model of the sub-basin of Chalco , Mexico. Phys. Earth Planet. Inter. 300, 106426. https://doi.org/10.1016/j.pepi.2020.106426

Vijayan, A., Agrawal, M., Gupta, R.K., 2022. Seismic Site Characterization Using Ambient Noise and Earthquake HVSR in the Easternmost Part of Shillong Plateau, India. J. Geol. Soc. India 98, 471–478. https://doi.org/10.1007/s12594-022-2004-3

Weydt, L.M., Lucci, F., Lacinska, A., Scheuvens, D., Carrasco-Núñez, G., Giordano, G., Rochelle, C.A., Schmidt, S., Bär, K., Sass, I., 2022. The impact of hydrothermal alteration on the physiochemical characteristics of reservoir rocks: the case of the Los Humeros geothermal field (Mexico), Geothermal Energy. Springer Berlin Heidelberg. https://doi.org/10.1186/s40517-022-00231-5

Winkens, G., Kauffmann, A., Herrmann, J., Czerny, A.K., Obert, S., Seils, S., Boll, T., Baruf, C., Rao, Y., Curtin, W.A., Schwaiger, R., Heilmaier, M., 2026. in Mo-Ti alloys. Commun. Mater. 4(1), 1–10. https://doi.org/10.1038/s43246-023-00353-8

Yulianur, A., Saidi, T., Setiawan, B., Sugianto, S., Rusdi, M., 2020. Microtremor measurement at liquefaction-induced Ground Deformation Area. J. Eng. Sci. Technol. 15, 2871–2889.

Zaenudin, A., Darmawan, I.G.B.O.Y., Wibowo, R.C., 2022. Shear wave velocity estimation based on the particle swarm optimization method of HVSR curve inversion in Bakauheni district , Indonesia 31, 480–493. https://doi.org/10.55730/1300-0985.1815

Zhang, J., Kato, A., Dindar, A.A., 2025. Structure Heterogeneity Around the Western End of the 1999 Izmit Earthquake Rupture Revealed by Distributed. https://doi.org/10.1029/2025GL116809

Zhang, S., Chen, M., Zhang, W., Zhuang, X., 2019. Highlights. Expert Syst. Appl. 113123. https://doi.org/10.1016/j.eswa.2019.113123

Zhao, W., An, M., Zilio, L.D., Zhao, L., Gan, Q., Zhang, F., Elsworth, D., 2025. Coupled evolution of seismicity and permeability in fault zones.

Zhu, C., Cotton, F., Pilz, M., 2020. Detecting site resonant frequency using HVSR: Fourier versus response spectrum and the first versus the highest peak frequency. Bull. Seismol. Soc. Am. 110, 427–440. https://doi.org/10.1785/0120190186